HHS Public Access

Author manuscript

*Cell Rep*. Author manuscript; available in PMC 2020 January 02.

Published in final edited form as:

*Cell Rep*. 2019 October 01; 29(1): 76–88.e7. doi:10.1016/j.celrep.2019.08.076.

# Liver-Type Glutaminase GLS2 Is a Druggable Metabolic Node in Luminal-Subtype Breast Cancer

**Michael J. Lukey**[1,8], **Ahmad A. Cluntun**[2,3,6,8], **William P. Katt**[1,8], **Miao-chong J. Lin**[1,7], **Joseph E. Druso**[1,7], **Sekar Ramachandran**[2], **Jon W. Erickson**[2], **Henry H. Le**[2,5], **Zhihan-Emily Wang**[1], **Bryant Blank**[4], **Kai Su Greene**[1], **Richard A. Cerione**[1,2,9,*]

[1]Department of Molecular Medicine, Cornell University, Ithaca, NY 14853, USA

[2]Department of Chemistry and Chemical Biology, Cornell University, Ithaca, NY 14853, USA

[3]Graduate Field of Biochemistry, Molecular and Cell Biology, Cornell University, Ithaca, NY 14853, USA

[4]Department of Biomedical Sciences, Cornell University, Ithaca, NY 14853, USA

[5]Boyce Thompson Institute, Ithaca, NY 14853, USA

[6]Present address: Department of Biochemistry, University of Utah School of Medicine, Salt Lake City, UT 84112, USA

[7]Present address: Department of Pathology and Laboratory Medicine, University of Vermont, Burlington, VT 05405, USA

[8]These authors contributed equally

[9]Lead Contact

## SUMMARY

Efforts to target glutamine metabolism for cancer therapy have focused on the glutaminase isozyme GLS. The importance of the other isozyme, GLS2, in cancer has remained unclear, and it has been described as a tumor suppressor in some contexts. Here, we report that GLS2 is upregulated and essential in luminal-subtype breast tumors, which account for >70% of breast cancer incidence. We show that GLS2 expression is elevated by GATA3 in luminal-subtype cells but suppressed by promoter methylation in basal-subtype cells. Although luminal breast cancers resist GLS-selective inhibitors, we find that they can be targeted with a dual-GLS/GLS2 inhibitor.



*Correspondence: rac1@cornell.edu.

AUTHOR CONTRIBUTIONS

Conceptualization, R.A.C., M.J.L., W.P.K., and A.A.C.; Methodology, R.A.C., M.J.L., W.P.K., and A.A.C.; Investigation, M.J.L., A.A.C., W.P.K., M.-c.J.L., J.E.D., B.B., J.W.E., S.R., H.H.L., Z.-E.W., and K.S.G.; Writing—Original Draft, M.J.L., A.A.C., W.P.K., and R.A.C.; Writing—Review and Editing, M.J.L., A.A.C., W.P.K., M.-c.J.L., J.E.D., S.R., J.W.E., H.H.L, Z.-E.W., B.B., K.S.G., and R.A.C.; Funding Acquisition, R.A.C., M.J.L., and A.A.C.

SUPPLEMENTAL INFORMATION

Supplemental Information can be found online at https://doi.org/10.1016/j.celrep.2019.08.076.

DECLARATION OF INTERESTS

The authors declare no competing interests.

These results establish a critical role for GLS2 in mammary tumorigenesis and advance our understanding of how to target glutamine metabolism in cancer.

## Graphical Abstract

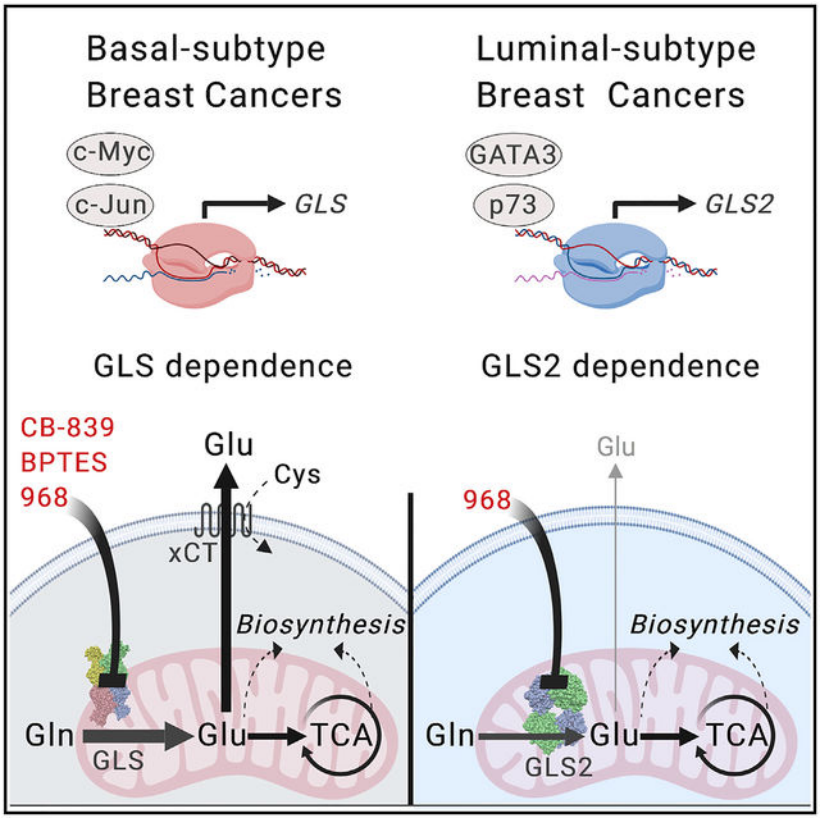


## In Brief

Lukey et al. report that basal- and luminal-subtype breast cancers employ different strategies for glutamine catabolism, impacting their sensitivity profiles to glutaminase inhibitors. Elevated GLS2 expression in luminal-subtype cancers is driven in part by GATA3. Targeting GLS2 with the pan-glutaminase inhibitor 968 inhibits luminal-subtype breast cancer cell proliferation and tumorigenesis.

## INTRODUCTION

Sustained biomass accumulation in tumors depends on cancer cells acquiring nutrients from the environment and processing them to meet the biosynthetic, bioenergetic, and redox demands of proliferation (Pavlova and Thompson, 2016). Many oncogenic signaling pathways regulate the expression, activity, or localization of nutrient transporters and metabolic enzymes, and extrinsic factors such as $O_2$ availability also influence cellular metabolism (Vander Heiden and DeBerardinis, 2017). These variables cause cancer cell metabolism to be highly heterogeneous in nature, although certain metabolic alterations are consistently observed in diverse tumor types. For example, most tumors exhibit elevated

glucose uptake coupled to lactate secretion regardless of $O_2$ availability (the Warburg effect), and cancer cells also frequently depend on an exogenous supply of glutamine (Pavlova and Thompson, 2016).

Glutamine is the most abundant amino acid in blood serum and is a major source of carbon and nitrogen for tumor cells. Its uptake into cells is facilitated by plasma membrane transporters, which in some cases are essential for tumorigenesis (van Geldermalsen et al., 2016). Once in the cytosol, there are several possible fates for glutamine in addition to its role as a proteinogenic amino acid. In mitochondria, glutamine catabolism is initiated by glutaminase, which releases the amide nitrogen as ammonia to generate glutamate. In turn, glutamate can be incorporated into the glutathione and proline biosynthesis pathways, or deaminated to produce the tricarboxylic acid (TCA) cycle intermediate α-ketoglutarate (α-KG). This metabolic pathway is widely upregulated in cancer cells, with glutamine serving as a key anaplerotic substrate for the TCA cycle (Cluntun et al., 2017).

Two genes encode glutaminases in mammals, *GLS* and *GLS2*, and different isoforms of each enzyme arise from alternative splicing and surrogate promoter mechanisms (Katt et al., 2017). The GLS isozyme is ubiquitous in healthy tissues, whereas liver-type glutaminase (GLS2) is restricted primarily to the liver, pancreas, and brain (Altman et al., 2016). Expression of GLS is regulated by oncogenic transcription factors, and its role in cancer is well characterized and supportive of tumorigenesis (Gao et al., 2009; Lukey et al., 2016). Consequently, GLS has been investigated as a possible drug target for cancer therapy, and an allosteric inhibitor, CB-839, is currently being evaluated in clinical trials (Gross et al., 2014). The function of GLS2 in cancer is less well defined and appears to be context dependent. The *GLS2* gene is a transcriptional target of p53 (Hu et al., 2010; Suzuki et al., 2010), and in glioblastoma and liver cancer GLS2 has been described as a tumor suppressor (Matés et al., 2018). However, *GLS2* expression is also regulated by oncoproteins including N-myc (Xiao et al., 2015) and was identified as one of only 16 essential metabolic genes for tumorigenesis in a functional genomics screen (Possemato et al., 2011).

Here, we describe a critical onco-supportive role for GLS2 in breast cancer. We demonstrate that expression of the *GLS2* gene is regulated by GATA3 and that the gene product is essential for cell proliferation and tumorigenesis in luminal-subtype breast cancers, which account for ~75% of total breast cancer incidence (Table S1) (Dai et al., 2015). Moreover, we show that GLS2 can be targeted with the small-molecule inhibitor 968 to suppress tumorigenesis and overcome resistance to GLS-selective inhibitors. These findings establish a previously unappreciated essential role for GLS2 in breast cancer biology and provide important insights regarding how to target glutamine metabolism for cancer therapy.

## RESULTS

### Luminal Breast Cancers Use Glutamine Anaplerosis but Resist GLS Inhibitors

The most extensively studied inhibitors of GLS are based on the bis-2-(5-phenylacetamido-1,3,4-thiadiazol-2-yl) ethyl sulfide (BPTES) molecular scaffold, with the potent analog CB-839 currently in clinical trials for a number of malignancies. CB-839 was originally reported to be effective against triple-negative breast cancer (TNBC) cells (Gross

et al., 2014), which are characterized by low expression of the receptors estrogen receptor (ER), progesterone receptor (PR), and HER2. Across a collection of breast cancer cell lines, we observed that basal-subtype cells respond to BPTES or CB-839 treatment, whereas luminal-subtype cells resist these inhibitors, regardless of their specific receptor status (Figure 1A; Tables S2 and S3). We previously reported the same selectivity profile for the related inhibitor UPGL00004, indicating that this entire class of molecules is ineffective against luminal-subtype breast cancers (Huang et al., 2018).

However, the sensitivity of breast cancer cells to GLS inhibitors does not correspond to their rate of glutamine consumption or to their expression of SLC1A5 (Figures 1B and 1C), the major facilitator of glutamine uptake in breast cancer (van Geldermalsen et al., 2016). We therefore used stable isotope tracing to determine the fate of glutamine-derived carbon in the different breast cancer subtypes (Figure S1A). Cells were cultured in medium containing uniformly labeled $^{13}$C-glutamine for 10 h, and metabolites were then extracted for analysis by liquid chromatography-high-resolution mass spectrometry (LC-HRMS). In both basal-subtype (MDA-MB-231 and TSE) and luminal-subtype (T-47D and MDA-MB-453) cells, glutamine is a major source of carbon for the TCA cycle (Figure 1D). The proportion of the TCA cycle intermediates α-KG and fumarate derived directly from [U-$^{13}$C]-glutamine (i.e., the abundance ratio of m+5 α-KG and m+4 fumarate) ranges from ~30% to ~55%. The abundance ratio of m+4 citrate ranges from 18% to 35%, whereas only trace quantities of m+5 citrate are present in all cell lines, indicating that the TCA cycle is turning in the oxidative direction under the aerobic experimental conditions. The abundance of TCA cycle metabolites showed no consistent differences between luminal- and basal-subtype cells (Figure S1B), and samples collected at different time points (1 h, 24 h) had similar labeling patterns to those collected at 10 h (Figure S1C). Thus, both luminal- and basal-subtype breast cancer cells make use of glutamine as an anaplerotic substrate, despite their contrasting sensitivity to GLS inhibitors.

## Expression of GLS2 Is Elevated in Luminal-Subtype Breast Cancers

Previously, the glutaminase isozyme GLS2 has been described as a tumor suppressor in some contexts, with downregulated expression in liver and brain cancers (Matés et al., 2018). However, since luminal-subtype breast cancer cells resist GLS inhibitors yet still exhibit glutamine-mediated anaplerosis, we hypothesized that they might instead be dependent on GLS2. We used The Cancer Genome Atlas (TCGA) invasive breast cancer dataset (Koboldt et al., 2012) to examine *GLS2* transcript levels in the breast cancer molecular subtypes luminal A (LumA), luminal B (LumB), HER2$^+$, and basal. Expression of *GLS2* is indeed substantially higher in LumA and LumB tumors than in basal-subtype tumors, which instead have high levels of the *GLS* transcript (Figure 2A).

To compare protein levels of GLS2 in breast tumors and normal mammary tissue, we probed a tissue microarray (Figures 2B, 2C, and S2A). This revealed that GLS2 levels are significantly upregulated in receptor-positive breast tumors (the majority of which are luminal subtype) relative to normal tissue but are elevated only in a small number of receptor-negative breast tumors (generally basal subtype), with the mean level not differing significantly from normal tissue (Figure 2B). Microscopic examination of the stained tissue

slices revealed that in receptor-positive tumors, GLS2 is much more abundant in carcinoma cells than in neighboring connective tissue (Figure 2C). We then confirmed that the expression patterns for GLS and GLS2 are conserved in breast cancer cell lines. Quantitative real-time PCR analysis showed that the *GLS2* transcript is up to ~2,000-fold more abundant in luminal-subtype than in basal-subtype cells, which predominantly express *GLS* (Figures 2D and 2E). These differences are conserved at the protein level (Figure 2F). Consistent with other reports (Muir et al., 2017; Shin et al., 2017), high levels of GLS in basal-subtype cells are associated with expression of the glutamate/cystine antiport system "xCT" and corresponding rapid glutamate efflux (Figures S2B and S2C).

## GLS2 Is Localized to Mitochondria in Breast Cancer Cells

Although GLS2 contains a predicted mitochondrial localization signal (Katt et al., 2017), several subcellular localizations have been reported, including the nucleus in neurons and astrocytes and as a binding partner of the plasma membrane/cytosolic protein Rac1 in liver cancer cells (Cardona et al., 2015; Zhang et al., 2016). To establish the localization of GLS2 in breast cancer cells, we fractionated both MDA-MB-453 (high-GLS2) and MDA-MB-231 cells (high-GLS) and performed western blot analysis on the whole-cell lysates along with the cytosolic, mitochondrial, and nuclear fractions. As markers for these fractions, we also probed for the cytosolic enzyme asparagine synthetase (ASNS), the mitochondrial voltage-dependent anion channel (VDAC), and the nuclear envelope protein lamin A. Both GLS2 and GLS, along with VDAC, were detected almost exclusively in the mitochondrial fractions of both cell lines (Figure 2G). A small proportion of each glutaminase was present in the nuclear fractions, but the similar pattern for VDAC suggests that these signals arise from small quantities of mitochondria co-pelleting with nuclei (Figure 2G). As expected, ASNS was detected in the cytosolic fraction, and lamin A in the nuclear fraction (Figure 2G). We also examined the subcellular localization of ectopically expressed GLS2 using immunofluorescence. Supporting a mitochondrial localization for GLS2 in breast cancer cells, GLS2-HA co-localizes with the endogenous mitochondrial marker protein Hsp60 in SK-BR-3 cells, as well as with ectopically expressed GLS-myc (Figure S2D).

## GLS2 Expression Is Regulated by GATA3 and Promoter Methylation

To understand the upregulation of GLS2 in luminal-subtype breast cancers, we next investigated the mechanisms influencing *GLS2* gene expression. Data from TCGA show a high frequency of copy number gains at the *GLS2* gene locus in luminal-subtype and $HER2^+$ breast tumors (as high as 37% copy number gain, 2% gene amplification, in the case of LumB), but not in basal-subtype tumors (Figure S3A). The *GLS* locus exhibits the reverse pattern, with frequent copy number gains in basal-subtype and $HER2^+$ breast tumors, but not in LumA or LumB (Figure S3A). The transcription factors p53, p63, p73, c-Myc, and N-myc have each been shown to regulate *GLS2* expression in different contexts (Katt et al., 2017). However, we found that none of these regulators correlates with the pattern of GLS2 expression in breast cancer cells (Figure 3A), and we note that the *TP53* gene encoding p53 is mutated in BT-474, T-47D, MDA-MB-231, Hs 578T, and HCC38 cells. We therefore investigated whether additional factors contribute to the regulation of GLS2 expression in breast cancer.

Across the cell lines, there is no clear association between GLS2 levels and any one of the receptors ER, PR, or HER2, with MDA-MB-453 cells, which have low expression of all three receptors, having the highest GLS2 levels (Figure 3B). Since GLS2 is so abundant in LumA and LumB breast cancers relative to other subtypes, we wondered whether its expression is intrinsically associated with luminal cell status. Levels of GLS2 in breast cancer cell lines correlate closely with that of full-length GATA3 (Figure 3B), a "master regulator" of luminal differentiation (Asselin-Labat et al., 2007). There is also a strong positive correlation between *GATA3* and *GLS2* transcript levels in human breast tumors (Figure 3C). We therefore used PROMO (Farré et al., 2003; Messeguer et al., 2002) to analyze the human *GLS2* gene promoter, and identified a match to the GATA3 consensus motif at position −1,259 base pairs (bp) relative to the transcription start site (TSS) (Figure S3B). The probability of this sequence occurring randomly within 1,500 bp of the TSS is predicted by PROMO to be only 2.8%. We next carried out a chromatin immunoprecipitation (ChIP), pulling down GATA3 from cross-linked chromatin prepared from MDA-MB-453 cell nuclei and using quantitative real-time PCR to quantify a 176-bp stretch of the *GLS2* promoter centered on the GATA3 consensus motif. The GATA3 pull-down yielded a ~6-fold higher signal relative to input than a negative-control IgG IP, consistent with direct binding of GATA3 to this region of the promoter (Figure 3D). Finally, we knocked down GATA3 in MDA-MB-453 and T-47D cells and found that, after 48 h, this resulted in a corresponding decrease in GLS2 levels in each cell line (Figures 3E and S3D). Thus, GATA3 contributes to the elevated expression of GLS2 in luminal-subtype breast cancers.

Because GLS2 levels are so low in basal-subtype breast cancers, we also tested whether expression is epigenetically silenced in these cells via methylation of the *GLS2* gene promoter. After isolating genomic DNA from the basal-subtype cell lines with the lowest levels of *GLS2* transcript (TSE and Hs 578T) and the luminal-subtype cell lines with the highest levels (T-47D and MDA-MB-453), we used the MassARRAY system to quantify methylation levels at sites in the CpG island centered on the TSS of the *GLS2* gene (Figures S3B and S3C). In MDAMB-453 cells, which have the highest levels of GLS2, there is minimal promoter methylation, whereas in TSE cells, which have the lowest levels of *GLS2* transcript, almost every site within the CpG island has a high methylation ratio (Figure 3F). Treatment of TSE cells with the DNA hypomethylating agent azacitidine for 48 h resulted in increased GLS2 protein levels (Figure 3G). Collectively, these results show that GLS2 expression is regulated by GATA3 in luminal-subtype breast cancers, and potentially also by copy number gains, whereas expression in basal-subtype breast cancers is repressed by promoter methylation.

## GLS2 Mediates Glutamine Anaplerosis in Luminal-Subtype Cells

To probe the role of GLS2 in luminal-subtype cells, we asked whether GLS2 is involved in the observed supply of glutamine-derived carbon to the TCA cycle (Figure 1D). For comparison, we also quantified the anaplerotic role of GLS in basal-subtype breast cancer cells. We transduced MDA-MB-453 (luminal, high-GLS2) or MDA-MB-231 (basal, high-GLS) cells with constructs for expressing a control short hairpin RNA (shRNA) or shRNAs targeting GLS2 or GLS. After 48 h, we confirmed knockdowns using western blot analysis,

and observed that within this time frame there was no compensatory upregulation of the other glutaminase isozyme (Figure 4A). We then performed metabolomics experiments to assess the effects of the knockdowns on TCA cycle anaplerosis. Importantly, knockdown of GLS2 strongly inhibited glutamine-mediated TCA cycle anaplerosis in MDA-MB-453 cells (Figure 4B). As expected, knockdown of GLS in MDA-MB-231 cells also suppressed the delivery of carbon from [U-$^{13}$C]-glutamine into the TCA cycle (Figure 4B). The glutaminase knockdowns also decreased the total abundance of glutamate and TCA cycle intermediates (Figure S4A). As a control, we carried out the reciprocal experiment, treating MDA-MB-453 cells with GLS-targeted shRNAs, and MDA-MB-231 cells with GLS2-targeted shRNAs. In each case, the abundance of glutamate and TCA cycle metabolites was minimally perturbed (Figure S4B), further demonstrating that GLS2 is the predominant glutaminase in MDA-MB-453 cells and that GLS is the primary isozyme in MDA-MB-231 cells. Collectively, these findings establish that GLS2 is a metabolically active mitochondrial enzyme, critical for glutamine-mediated anaplerosis in luminal-subtype breast cancer cells.

## GLS2 Is Essential in Luminal-Subtype Breast Cancer

Cells Because various functions have been reported for GLS2 in cancer, including tumor-suppressive activity in liver cancer and glioblastoma (Matés et al., 2018), we next investigated the importance of GLS2 for breast cancer cell proliferation and tumorigenesis. We transfected luminal- and basal-subtype cell lines with either a control small interfering RNA (siRNA) or siRNAs selectively targeting GLS2, GLS, or both isozymes simultaneously. Western blot analysis 48 h after transfection confirmed that potent and selective knockdowns had been achieved (Figure 4C, lower panels). We then measured cell proliferation over 6 days. Knockdown of GLS2 strongly suppressed proliferation of luminal-subtype cells (MDA-MB-453 and T-47D), but only modestly impacted proliferation of basal-subtype cells (MDA-MB-231 and TSE) (Figure 4C, upper panels). Knockdown of GLS had no effect on luminal-subtype cells but did inhibit basal-subtype cells, consistent with the results using GLS-selective inhibitors (Figure 1A). In all cases, the effects of GLS2 and/or GLS knockdowns could be rescued by supplementation of the culture medium with 2 mM dimethyl α-KG (dm-α-KG) (Figure S4C), confirming that suppressed proliferation was a result of impaired TCA cycle anaplerosis.

We next addressed the importance of GLS2 for luminal-subtype breast tumor growth *in vivo*. This experiment required stable rather than transient depletion of GLS2, but potent shRNA-mediated knockdowns severely impacted luminal-subtype cell viability after several days. We therefore used a low titer of virus for transducing MDA-MB-453 cells and generated stable GLS2 partial-knockdown cell lines (Figure 4D). Proliferation of the GLS2 partial-knockdown cells in culture was 40%–50% slower than that of cells expressing a control shRNA (Figure 4E, left panel), and could be rescued with 2 mM dm-α-KG (Figure 4E, right panel). We then injected $3 \times 10^6$ control or GLS2 partial-knockdown cells, in Matrigel suspension, into each flank of female NOD.Cg-*Prkdc*$^{scid}$ *Il2rg*$^{tm1Wjl}$/SzJ (NSG) mice, and measured tumor growth over 42 days (n = 6 tumors per condition). Both tumor initiation time and the rate of tumor growth were strongly inhibited in the GLS2 partial-knockdown samples relative to the control, providing a proof of principle that targeting GLS2 can inhibit

luminal-subtype breast cancer tumorigenesis *in vivo* as well as cell proliferation *ex vivo* (Figure 4F).

## GLS2 Mediates Resistance to GLS Inhibitors

The BPTES class of inhibitors has been extensively studied and is highly selective for GLS over GLS2 (Figures S5A and S5B) (Robinson et al., 2007). Since GLS2 is capable of mediating TCA cycle anaplerosis in breast cancer cells, we tested whether it is sufficient to confer resistance to these inhibitors. We began by looking at the inhibition of glutaminase activity in isolated mitochondria. In mitochondria from luminal-subtype breast cancer cells, glutaminase activity was only partially inhibited by addition of 10 μM BPTES (Figure 5A). In the case of MDA-MB-453 cells, BPTES treatment had no effect on activity. As expected, for mitochondria isolated from basal-subtype cells, glutaminase activity was almost completely abolished by 10 μM BPTES (Figure 5A).

To gain further insight into the glutaminase expression profiles of breast cancer cells, we performed western blot analyses using known amounts of purified, recombinant GLS and GLS2 to estimate absolute levels of each glutaminase in cells (Figure S5C). We found that MDA-MB-453 cells contain ~275 pg of GLS2 per μg of total cellular protein and ~75 pg/μg GLS. In contrast, MDA-MB-231 cells contain ~500 pg/μg GLS and <75 pg/μg GLS2 (Figure S5C). In T-47D cells, the absolute levels of GLS and GLS2 are approximately equal, at ~200 pg/μg (Figure S5C). However, GLS requires much higher concentrations of inorganic phosphate (Pi) to reach maximal activity (Figure 5B), and in contrast to GLS2, its enzymatic activity is inhibited by its product, glutamate (Watford, 1993). At physiological mitochondrial Pi concentrations of ~10 mM (Hutson et al., 1992; Rauch et al., 1994), only GLS2 is fully activated (Figure 5B).

We next treated cells with 10 μM BPTES in culture medium containing [U-$^{13}$C]-glutamine and extracted and analyzed cellular metabolites. Consistent with the data above, BPTES treatment potently inhibited the supply of glutamine-derived carbon to glutamate and the TCA cycle in the basal-subtype cell lines Hs 578T and MDA-MB-231 (Figure 5C). In luminal-subtype MCF7 cells, which express GLS2 as well as GLS, BPTES treatment partially blocked glutamine anaplerosis (Figure 5C). In MDA-MB-453 cells, which express primarily GLS2, BPTES treatment had no impact on glutamine-mediated anaplerosis (Figure 5C). A similar pattern can be seen in the total abundances of TCA cycle intermediates (Figure S5D).

Using MDA-MB-231 and TSE cells, which express almost exclusively GLS, we generated derivative cell lines that ectopically express GLS2 (Figure 5D). In both cases, the clone with highest GLS2 expression showed a moderate decrease in the level of GLS. Although forced overexpression of GLS2 hinders the growth of liver cancer cells (Hu et al., 2010; Suzuki et al., 2010), in basal-subtype breast cancer cells each of the GLS2-overexpressing clones proliferated slightly more rapidly than control cells (Figure S5E). Ectopic expression of GLS2 greatly decreased sensitivity to BPTES treatment, with the $EC_{50}$ shifting to >20 μM for both cell lines, which matches the aqueous solubility limit of the inhibitor (Figure 5E; Table S4).

We then searched for basal-subtype breast cancer cells that are intrinsically resistant to GLS-selective inhibitors, to test whether resistance can be overcome by simultaneously targeting GLS2. The triple-negative, basal-subtype breast cancer cell line DU4475, which was originally derived from a metastatic lesion, is highly resistant to BPTES treatment, with an $EC_{50}$ value of >20 μM (Figure 5F). Western blot analysis showed that DU4475 cells express higher levels of GLS than MDA-MB-231 cells, but simultaneously express higher levels of GLS2 than MDA-MB-453 cells (~750 pg/mg of cellular protein for GLS, and ~625 pg/mg for GLS2) (Figures 5G and S5C). Knockdown of either glutaminase isozyme alone did not impact DU4475 cell proliferation, but simultaneous knockdown of both GLS and GLS2 significantly inhibited growth (Figures 5H and S5F). Proliferation was again restored by supplementation of the culture medium with 2 mM dm-α-KG (Figure S5G).

## 968 Inhibits GLS2 and Suppresses BPTES-Resistant Breast Cancer Growth

Previously, we reported that the small molecule 968 binds and inhibits the GLS splice variant GAC (Wang et al., 2010). This inhibitor has a much higher affinity for monomeric GAC than for the active tetramer and is proposed to bind to newly synthesized enzyme monomers and prevent the formation of activated tetramers (Stalnecker et al., 2015). However, the sensitivity of GLS2 to 968 has not previously been tested. We therefore measured the effect of 968 on the activity of purified, recombinant, glutaminase. In contrast to BPTES-class inhibitors, which are highly selective for GLS, 968 inhibited both GLS and GLS2, with a moderate (>3-fold) selectivity for GLS2 (Figure 6A). Compound 26, a quinoline derivative of 968 that differs by only a single carbon-to-nitrogen substitution, has greatly weakened affinity for GLS (Katt et al., 2012; Stalnecker et al., 2015). Similarly, we found that compound 26 minimally inhibits recombinant GLS2 at 50 μM, whereas 968 completely blocks activity at this concentration (Figure S6A).

Treatment of breast cancer cells with 968 inhibited proliferation with $EC_{50}$ values of 3–5 μM (Figure S6B; Table S4). For the cells with highest expression of GLS, maximal inhibition was ~70%–75%. The inactive analog compound 26 did not inhibit the proliferation of any of the cell lines we tested it against. Despite their intrinsic resistance to BPTES, DU4475 cells responded to 968 treatment with an $EC_{50}$ value of 4 μM (Figure 6B). We also measured the response of the GLS2-overexpressing derivatives of MDA-MB-231 and TSE cells, described above. Consistent with the ability of 968 to inhibit both glutaminase isozymes, overexpression of GLS2 had little effect on the $EC_{50}$ values for 968 (Table S4).

We next treated basal- and luminal-subtype breast cancer cells with 10 μM 968 and extracted metabolites for analysis at different time points. Consistent with the mechanism of 968 binding to monomeric glutaminase and preventing the formation of active tetramers, we observed a time-dependent inhibition of glutamine-mediated TCA cycle anaplerosis (Figure 6C). Matching the partial selectivity of 968 for GLS2 over GLS, the effects were more pronounced in MDA-MB-453 cells than MDA-MB-231 cells (Figure 6C). Treatment with 968 also decreased the total abundance of TCA cycle intermediates (Figure S6C).

Since 968 inhibits the proliferation of breast cancer cells *ex vivo* but does not affect the growth of primary human mammary epithelial cells or fibroblasts (Wang et al., 2010), we tested whether it can be used to treat luminal-subtype breast tumor growth *in vivo*. We

injected $3 \times 10^6$ MDA-MB-453 cells in Matrigel suspension into each flank of NSG mice (n = 6 xenografts per condition) and waited until palpable tumors 1–2 mm in diameter were present (14 days). At this point, mice were separated into two groups, with one group receiving subcutaneous injections of 968 (10 mg/kg body weight) 3 times per week, and the other group receiving carrier solution only. We continued to monitor tumor growth for 3 weeks after initiating treatment and found that it was robustly inhibited in 968-treated animals (Figure 6D). In contrast, treatment of animals with 10 mg/kg BPTES did not significantly impact tumor growth (Figure 6E). Thus, 968 inhibits GLS2 *in vitro*, suppresses GLS2-mediated anaplerosis, and is effective against BPTES-resistant breast cancer cell proliferation and tumorigenesis. Taken together, our results reveal an essential and potentially druggable role for GLS2 in luminal-subtype breast cancers.

## DISCUSSION

Efforts to target glutamine catabolism for cancer therapy have focused on inhibiting the glutaminase isozyme GLS, which is highly expressed and onco-supportive in diverse malignancies (Cluntun et al., 2017). The importance of the other mammalian glutaminase, GLS2, in tumorigenesis has remained less clear, and various subcellular localizations and functions have been described, including tumor suppressor activity (Matés et al., 2018). We report here that GLS2 is upregulated in luminal-subtype/receptor-positive breast cancers, where it is essential for glutamine-mediated TCA cycle anaplerosis, cell proliferation, and tumorigenesis. These findings explain the identification of GLS2 as one of only 16 metabolic enzymes required for tumorigenesis in an earlier functional genomics screen (Possemato et al., 2011).

Previous studies found that triple-negative, but not receptor-positive, breast cancer cell lines often express high levels of the GLS splice variant GAC (Gross et al., 2014). Our results indicate that, rather than being directly dictated by the cellular receptor status, differences in glutaminase expression in breast cancer correspond to the intrinsic molecular subtype (Figure 2). Specifically, LumA and LumB breast tumors display relatively high levels of GLS2, whereas GLS is elevated in basal-subtype breast tumors. Since expression of the *GLS2* gene is driven in part by the transcription factor GATA3 (Figure 3), a master regulator of luminal differentiation, high levels of GLS2 might be intrinsically associated with luminal cell status. Expression of both glutaminase isozymes is low in $HER2^+$ breast tumors, suggesting that glutaminase-mediated TCA cycle anaplerosis might not be a major metabolic pathway in this disease subtype.

Our findings highlight the importance of considering GLS2 when identifying target diseases for treatment with GLS-selective inhibitors. Gene expression data from TCGA show that *GLS2* transcript levels are consistently upregulated relative to healthy tissue in colorectal tumors and also in a subset of lung tumors. With clinical trials underway to evaluate the efficacy of CB-839 against these cancers, it will be important to characterize further the function of GLS2 in these contexts. In pancreatic ductal adenocarcinoma (PDAC) cells, GLS inhibitors have only a temporary cytostatic effect, which is followed by metabolic adaptation and recovery of proliferation (Biancur et al., 2017). Notably, GLS2 is present in both healthy pancreas and PDAC cells (Altman et al., 2016; Biancur et al., 2017), and thus might provide

a critical supply of glutamate following GLS inhibition. The sensitivity of some cancer cells to GLS inhibitors requires high expression of the xCT anti-porter, which exchanges intracellular glutamate for extracellular cystine and can therefore deplete intracellular glutamate reserves (Muir et al., 2017). Thus, a signature of concurrent high expression of GLS and xCT, along with low levels of GLS2, might identify tumors that are most likely to respond to GLS-targeted therapy.

### GLS2 as a Potential Therapeutic Target

In healthy tissues, GLS2 expression is highest in periportal regions of the liver, where it allows glutamine carbon to be directed via the TCA cycle into the gluconeogenic pathway in response to glucagon (Lacey et al., 1981; Watford and Smith, 1990). For GLS2 to be targeted for cancer therapy, any toxicity arising from inhibiting its normal physiological function must be within a tolerable range. We observed that mice treated with 968 at 10 mg/kg body weight, three times weekly for 3 weeks, showed no gross evidence of toxicity. Moreover, it was recently reported that *GLS2* knockout mice are viable, albeit with a decreased ability to maintain plasma glucose levels during fasting (Miller et al., 2018). These results indicate that GLS2 could be safely targeted as a strategy for treating luminal-subtype breast cancers, most likely as part of a combination therapy designed to maximize cancer cell dependence on the glutaminase reaction. To date, drug discovery efforts for blocking glutamine catabolism in cancer have focused almost exclusively on the GLS isozyme. However, a small number of molecular scaffolds have now been reported to inhibit GLS2 (Wu et al., 2018), including 968, which we show targets both isozymes with a moderate (~3-fold) selectivity for GLS2. Our finding that GLS2 is upregulated and essential in the most prevalent subtypes of breast cancer support the notion of building on these scaffolds to develop more potent inhibitors for selective targeting of GLS2-high cancers.

## STAR⋆METHODS

### LEAD CONTACT AND MATERIALS AVAILABILITY

Further information and requests for resources and reagents should be directed to and will be fulfilled by the Lead Contact, Richard A. Cerione (rac1@cornell.edu). Plasmids generated in this study are available from the Lead Contact without restriction.

### EXPERIMENTAL MODEL AND SUBJECT DETAILS

**Human Cell Lines—**Human breast cancer cell lines MCF7, BT-474, T-47D, MDA-MB-453, MDA-MB-231, Hs 578T, HCC38, SK-BR-3, and DU4475 were purchased from the American Type Culture Collection (ATCC) and no additional cell authentication was performed. The TSE human breast cancer cell line was supplied by Dr. Steven Abcouwer (University of Michigan). All breast cancer cells were cultured at 37°C under a 5% $CO_2$ atmosphere in RPMI 1640 medium containing 2 mM glutamine (GIBCO) and supplemented with 10% fetal bovine serum (FBS) (GIBCO). The 293T cell line (ATCC) used for generating lentivirus particles was cultured as above but using DMEM, high glucose (GIBCO).

**Animals—**All experiments involving mice were carried out according to protocols approved by the Institutional Animal Care and Use Committee at Cornell University. In all cases, 6–8 week old female NOD.Cg-*Prkdc*$^{scid}$ *Il2rg*$^{tm1Wjl}$/SzJ (NSG) mice (The Jackson Laboratory) were used. For xenograft experiments, a suspension of MDA-MB-453 breast cancer cells (or derivative cell lines stably expressing shRNAs) was mixed 1:1 with Matrigel Matrix (BD Biosciences) to give a final concentration of $3 \times 10^6$ cells per 100 μl, and $3 \times 10^6$ cells were immediately injected into each of the two flanks of 6–8 week old female NOD.Cg-*Prkdc*$^{scid}$ *Il2rg*$^{tm1Wjl}$/SzJ (NSG) mice (n = 3 mice per condition). Tumor sizes were measured using calipers, and estimated volumes were calculated using the formula $V = (\pi/6) \times \text{length} \times \text{width}^2$, as described previously (Tomayko and Reynolds, 1989). For experiments using MDA-MB-453 cells stably expressing shRNAs, mice were sacrificed after 6 weeks. For 968 treatment studies, when tumors of 1–2 mm diameter were detected, the mice were randomly divided into two groups and intraperitoneal (IP) injections of 968 (10 mg/kg) solution or carrier solution were initiated and carried out three times weekly. The formulation was prepared immediately prior to injection and consisted of 70% PBS, 20% Cremophor EL, 10% DMSO, and 968 diluted from a 21 mM DMSO stock. Mice were sacrificed after 3 weeks of treatment.

## METHOD DETAILS

**Cell Lysis and Western Blot Analysis—**Cells, or fractionated mitochondria and nuclei, were lysed with ice-cold lysis buffer (50 mM HEPES pH 8.0, 150 mM NaCl, 25 mM NaF, 1% (v/v) Triton X-100, 1 mM $MgCl_2$, 50 mM β-glycerophosphate, 30 μg/ml leupeptin, 5 μg/ml aprotinin), and insoluble debris cleared by centrifugation at 4°C. Protein concentrations were determined by Bradford assay (Bio-Rad), and lysate was then boiled for 10 min in reducing SDS-sample buffer. Lysate proteins (20 μg total protein/lane, except for the cell fractionation experiment in which 5 μg total protein/lane was used) were then resolved on Novex 12% Tris-Glycine Mini Gels (Thermo Fisher Scientific) and transferred to PVDF membrane (PerkinElmer). Membranes were blocked in 7% BSA in Tris-Buffered Saline plus 0.05% TWEEN 20 (TBST) for 1 h at room temperature and probed overnight at 4°C in primary antibody solution in TBST (see Table S5 for antibody dilutions). They were then washed with TBST and incubated in TBST containing 25% (v/v) non-fat dry milk powder and anti-Rabbit or anti-Mouse secondary antibody (1:2500) for 1 h. Finally, membranes were washed in TBST, and imaged using Western Lightning Plus-ECL (PerkinElmer) and HyBlot ES autoradiography film (Denville Scientific Inc.).

**Breast Tumor Tissue Microarray—**Tissue microarray BRC961 (US Biomax) was probed as follows, using the anti-GLS2 antibody (Abgent, AP6650D). Reagents were from Vector Laboratories VECTASTAIN Elite ABC HRP kit (Cat# PK-6200), Avidin/Biotin blocking kit (Cat# SP-2001), and ImmPACT DAB Peroxidase (HRP) Substrate (Cat# SK-4105). Deparaffinization was carried out by heating the slide to 60°C for 20 min and then immersing the slide in mixed xylenes (2 × 10 min), 100% ethanol, 95% ethanol, 70% ethanol (5 min each) and finally $H_2O$ (2 × 5 min). The antigen retrieval step involved immersing the slide in 10 mM sodium citrate buffer, pH 6.0 at ~95°C for 15 min and then cooling at room temperature for 20 min. To remove endogenous peroxidase the slide was washed with $H_2O$ (2 × 5 min) and then incubated in 3% $H_2O_2$ in $H_2O$ for 10 min. The slide

was then washed in $H_2O$ for 5 min followed by PBS for 5 min. Blocking was carried out at room temperature using horse serum (20 min), PBS rinse, avidin solution (15 min), PBS rinse, biotin solution (15 min), PBS rinse, followed by PBS washes (2 × 5 min). The slide was then incubated overnight at 4°C with the anti-GLS2 primary antibody (1:100 in horse serum). Next, the slide was washed with PBS (4 × 5 min), incubated for 30 min at room temperature with biotinylated universal secondary antibody, and washed again with PBS (4 × 5 min). Then, the slide was incubated for 30 min at room temperature with VECTASTAIN ABC reagent and washed again with PBS (4 × 5 min). To develop, the slide was incubated with diluted ImmPACT DAB chromogen for ~2 min and then washed in $H_2O$ (2 × 5 min). Finally, the stained slide was dehydrated by immersing in 70% ethanol, 95% ethanol, 100% ethanol (5 min each) and mixed xylenes (2 × 5 min), mounted using Permount mounting medium (Fisher) and sealed. Signal intensity was quantified using ImageJ. Receptor staining intensity data were from US Biomax.

**RNA Isolation and Quantitative Real-Time PCR—**Total RNA was extracted from cells using the RNeasy Mini Kit (QIAGEN) and QIAshredder (QIAGEN), and cDNAs were prepared using SuperScript III Reverse Transcriptase (Thermo Fisher Scientific). RT-PCR was carried out using the 7500 fast real-time PCR system (Applied Biosystems), using appropriate primers (Table S6) with cDNA as the template. In all cases, 18S rRNA served as the endogenous control. All primer sequences were obtained from PrimerBank (https://pga.mgh.harvard.edu/primerbank/), and primers were synthesized by Integrated DNA Technologies. Reactions were carried out using Power SYBR Green PCR Mix (Thermo Fisher Scientific).

**Genomic DNA Isolation and DNA Methylation Analysis—**High molecular weight genomic DNA was isolated from breast cancer cells using QIAamp DNA Mini Kit (QIAGEN), and contaminating RNA was digested using RNase One Ribonuclease (Promega) followed by re-purification of DNA, elution with water, and adjustment of DNA concentration to 50 ng/μl. To assess DNA purity, UV/visible absorption spectra were measured, and for all samples the A260/280 ratio was >1.7 and the A260/230 ratio was >2.0. Samples were then submitted to the Epigenomics Core at Weill Cornell Medical College, where bisulfite conversion was carried out followed by DNA methylation analysis using Mass ARRAY EpiTYPER1.2 Suite (Agena Bioscience). The sequence of the CpG island in the *GLS2* gene promoter was obtained from human reference genome GRCh38/hg38 using the UCSC Genome Browser (https://genome.ucsc.edu). Primers for DNA methylation analysis were designed using EpiDesigner (Agena Bioscience) and synthesized by Integrated DNA Technologies (Table S6). Relative methylation ratios at CpG sites are presented as a heatmap, generated using MORPHEUS (https://software.broadinstitute.org/morpheus).

**Immunofluorescence—**Cells were fixed with 3.7% formaldehyde in PBS for 20 min and then permeabilized with PBS containing 0.1% Triton X-100 (v/v) for 20 min. Samples were blocked with 10% BSA (w/v) in PBS for 1 h, rinsed with PBS and then incubated with primary antibody in PBS containing 5% BSA (w/v) for 2 h. Samples were washed 3 times with PBS, and then Texas Red- or Oregon Green 488-conjugated secondary antibody diluted 1:400 in PBS containing 5% BSA (w/v), along with DAPI counterstain, was added for 1 h.

Samples were washed 3 times with PBS, mounting medium was applied, and slides were sealed with a coverslip prior to imaging with a ZEISS Axioscope.

**Cell Fractionation and Mitochondrial Isolation—**Breast cancer cells were fractionated into cytosolic, mitochondrial, and nuclear components via partial lysis and centrifugation using the Qproteome Mitochondria Isolation Kit (QIAGEN). For all samples, a portion of the starting material (i.e., whole cells) was retained for comparison with the isolated fractions. When cellular fractions were to be analyzed only by western blot, a single 10 cm dish of exponentially growing cells was used. When mitochondria were isolated for glutaminase assays, two 15 cm dishes of exponentially growing cells were used.

**Mitochondrial Glutaminase Activity Assays—**A two-reaction protocol was used to measure mitochondrial glutaminase activity. Mitochondria (5 μg total protein) were added to 105 μL of Reaction Mix 1 (20 mM glutamine, 0.2 mM EDTA, 50 mM Tris-acetate pH 8.6), supplemented with 10 μM BPTES when appropriate, and samples were incubated at 37°C for 40 min. The reaction was then quenched by addition of 10 μL of 2.4 M HCl, and samples placed on ice. Next, 20 μL of quenched Reaction Mix 1 was added to 200 μL of Reaction Mix 2 (1 unit bovine liver glutamate dehydrogenase (Sigma-Aldrich), 80 mM Tri-HCl pH 9.4, 200 mM hydrazine, 0.25 mM ADP, 2 mM NAD) and samples were incubated for 1 h at room temperature. The absorbance at 340 nm was then measured against a matched sample in which heat-inactivated mitochondria (immersed in boiling water for 5 min) were used. A standard curve was prepared using given concentrations of glutamate in Reaction Mix 2, allowing the amount of glutamate produced in Reaction 1 to be determined.

**Real-Time Recombinant Glutaminase Activity Assays—**Real-time monitoring of glutaminase activity through NADH production was performed on a Cary Eclipse fluorescence spectrometer. The excitation and emission wavelengths were set at 340 nm and 460 nm, respectively. To a 1 mL cuvette, 900 μL of assay buffer was added, followed by 10 μL of GDH, 40 μL of 50 mM NAD and 20 μL of either DMSO or various dilutions of 968. Then, 100 μL of either 100 nM GAC or 500 nM GLS2 was added to this mixture and the fluorescence emission was monitored in real time. After 30 s, 200 μL of a mixture of glutamine and $K_2HPO_4$ was added such that the final concentrations of $K_2HPO_4$ and glutamine were 100 mM and 20 mM, respectively. The initial velocity of glutamine hydrolysis was obtained from the slopes of the linear portion of the kinetic curve.

**Glutamine Consumption and Glutamate Release Assays—**To 6-well plates containing 2 mL phenol red-free culture medium/well, $2 \times 10^5$ cells/well were added and incubated overnight to attach. Wells were then rinsed twice with serum-free, phenol red-free culture medium, and 2 ml/well fresh serum-free/phenol red-free medium (containing 2 mM glutamine) was added, followed by incubation for 19 h. As a negative control, wells containing culture medium only were used. Medium was then collected, cellular debris removed by centrifugation at 4°C, and the supernatant retained and stored on ice. Meanwhile, cells attached to the wells were lysed and total protein was quantified using the Bradford assay. Glutamine concentrations were determined using the L-Glutamine/ Ammonia Assay Kit (Rapid) (Megazyme) following the manufacturer's instructions. Briefly,

50 μL sample was mixed with 100 μL Assay Buffer 1 and 10 μL Glutaminase Suspension and incubated at room temperature for 5 min. For all reactions, a blank containing 50 μL $H_2O$ was run in parallel. Then, 150 μL Assay Buffer 2, 100 μL NADPH Solution, and $H_2O$ to bring the final volume to 1160 μL was added, followed by incubation at room temperature for 4 min. Absorbance $A_1$ was then measured at 340 nm. Next, 10 μL Glutamate Dehydrogenase Suspension was added, samples were mixed and incubated at room temperature for 5 min, and absorbance $A_2$ was measured at 340 nm. Sample concentrations of glutamine were calculated using the extinction coefficient of NADPH at 340 nm. Changes in sample glutamine concentrations were measured relative to the culture medium samples which had been incubated in cell-free wells. To measure glutamate levels in culture medium, samples were analyzed by Reaction 2 described above for the mitochondrial glutaminase activity assays.

**Cell Proliferation Assays—**Culture medium was added to 12-well plates (1 ml/well) and wells were seeded with cells at Day 0 as follows. MCF7, T-47D, BT-474, HCC38 cells: $2 \times 10^4$ cells/well. MDA-MB-453 and MDA-MB-231 cells: $1 \times 10^4$ cells/well. TSE and Hs 578T cells: $0.3 \times 10^4$ cells/well. After 16 h, culture medium was replaced with fresh medium supplemented with appropriate concentrations of inhibitors and was subsequently replaced every 48 h. On Day 6 cells were trypsinized and suspended in an appropriate volume of culture medium, and the total number of cells per well was determined using a hemocytometer or a TC20 Automated Cell Counter (Bio-Rad).

**DNA Constructs for Expressing GLS and GLS2—**Vectors for expressing human GAC or GLS2 in breast cancer cell lines were based on pCDNA3.1/V5-His TOPO (Thermo Fisher Scientific), with the appropriate gene sub-cloned in and the tag switched to HA-tag or myc-tag for immunofluorescence experiments. Vectors pQE80-GAC-72–598 and pQE80-GLS2-38-602, for expressing the processed forms of human GAC (residues 72 to 598) or GLS2 (residues 38 to 602) in *E. coli*, were described in Huang et al. (2018).

**Expression and Purification of Recombinant GAC and GLS2—**Recombinant GAC and GLS2 were expressed in *E. coli* as described in Huang et al. (2018). Briefly, *E. coli* strain BL21(DE3) (Thermo Fisher Scientific) were transformed with vector pQE80-GAC-72–598 or with pQE80-GLS2-38-602 to express the processed forms of GAC and GLS2, respectively. For both constructs, expression was induced with 0.3 mM IPTG for 20 h at 18°C, and cells were then harvested by centrifugation and lysed by sonication in binding buffer (500 mM NaCl, 50 mM Tris-HCl pH 8.5, 10 mM imidazole, 5 mM β-mercaptoethanol, 1 mM benzamidine chloride). The lysate was centrifuged, and the supernatant applied to a Ni-NTA column which was then washed with 100 column volumes of binding buffer followed by 10 volumes of wash buffer (500 mM NaCl, 50 mM Tris-HCl pH 8.5, 40 mM imidazole, 5 mM β-mercaptoethanol, 1 mM benzamidine chloride). Protein was eluted with 5 column volumes of elution buffer (500 mM NaCl, 300 mM imidazole-HCl pH 7.5, 5 mM β-mercaptoethanol, 1 mM benzamidine chloride). The eluate was centrifugally concentrated and then further purified by FPLC using a HiLoad 16/600 Superdex 200 column (GE Healthcare) with 150 mM NaCl, 5 mM Tris-HCl pH 7.5.

**Transfection of Breast Cancer Cells with DNA Constructs—**For 60 mm dish format. 0.2 mL Opti-MEM (GIBCO) containing 1.5 μg of the appropriate DNA construct, along with 0.2 mL Opti-MEM containing 12 μL Lipofectamine 2000 (Invitrogen), were separately incubated at room temperature for 5 min. The two solutions were combined and incubated for an additional 20 min, mixed with 1.6 mL culture medium and added to cells. After 5 h incubation at 37°C the transfection mixture was replaced with fresh culture medium, and cells were then incubated for an additional 48 h to allow for ectopic expression of GLS or GLS2. To select for cells stably expressing the DNA construct, culture medium supplemented with 500 μg/ml G-418 disulfate (Research Products International) was added and replaced every 2 days for 2–3 weeks until isolated colonies ~2 mm in diameter were present. Individual colonies were transferred to a 12-well plate (1 colony per well) using sterile blotting paper soaked in trypsin solution and were then cultured in medium supplemented with 250 μg/ml G-418 disulfate. All colonies were screened by western blot for ectopic expression, and positive clones were maintained in medium supplemented with 250 μg/ml G-418 disulfate.

**Genetic Knockdowns using siRNAs—**Transient knockdowns of GATA3, GLS, and GLS2 were achieved using two rounds of transfection with Silencer Select pre-designed siRNAs (Invitrogen). For 60 mm dish format, 0.3 mL Opti-MEM (GIBCO) containing 100 nM of the appropriate siRNA (to give a final siRNA concentration of 10 nM when diluted as below), along with 0.3 mL Opti-MEM containing 12 μL Lipofectamine 2000 (Invitrogen), were incubated separately at room temperature for 5 min. The two solutions were then combined and incubated for an additional 20 min, mixed with 2.4 mL culture medium, and added to cells. After 5 h incubation at 37°C the transfection mixture was replaced with fresh culture medium. For all knockdowns, two independent siRNAs were used, along with a negative control siRNA.

**Genetic Knockdowns using shRNAs—**The MISSION RNAi system (Sigma-Aldrich) was used for shRNA-mediated knockdown of GLS and GLS2. Lentivirus particles for each shRNA construct were generated using exponentially growing 293T cells (ATCC) as follows. For 10 cm dish format, 570 μL DMEM was mixed with 33 μL FuGENE 6 (Promega) and incubated at room temperature for 5 min. Plasmids pLKO.1-shRNA (5 μg), pCMV-dR8.2 (packaging vector) (5 μg), and pMD2.G (envelope vector) (1 μg) were then added to the solution, incubated for an additional 15 min, mixed with 8 mL culture medium and added to cells. Cells were incubated at 37°C overnight and the transfection medium was then replaced with fresh culture medium, followed by an additional 24 h incubation to allow for production of virus particles. Virus-containing medium was then collected, and cellular debris removed by centrifugation. To transduce breast cancer cells, virus-containing supernatant was diluted 1:12 in fresh culture medium, and 6 μg/ml polybrene was added before applying to cells. After 6 h incubation at 37°C the transduction medium was replaced with fresh culture medium, and cells were incubated for an additional 48 h before knockdowns were validated. For both GLS and GLS2 knockdowns, two independent shRNA constructs were used, and for all experiments the effects of knockdown were compared with those of a control shRNA. To select for stable expression of the constructs, cells were cultured in medium containing 0.5 μg/ml puromycin.

**Data from The Cancer Genome Atlas—**Gene expression data (RNA-Seq V2, RSEM) from TCGA invasive breast cancer dataset (Koboldt et al., 2012) were accessed using UCSC Xena (https://xena.ucsc.edu) or cBioPortal (http://www.cbioportal.org). Breast tumor subtype calls made by UCSC Xena were based on RNA-Seq data. Outlier readings are not shown on box and whisker plots but are included in calculation of the mean. Copy-number analysis data were accessed using cBioPortal.

**Metabolite Extraction—**The procedures for metabolite extraction from cultured cells are described in previous studies (Cluntun et al., 2015; Liu et al., 2014). Briefly, adherent cells were grown in 6-well plates in biological triplicate to 80% confluence, medium was rapidly aspirated and cells were washed with cold PBS on ice. Then, 1 mL of extraction solvent (80% methanol/water) cooled to −80°C was added to each well, and the dishes were transferred to −80°C for 15 min. Cells were then scraped into the extraction solvent on dry ice. All metabolite extracts were centrifuged at 20,000 × *g* at 4°C for 10 min. Finally, the solvent in each sample was evaporated in a Speed Vacuum. The cell extracts were dissolved in 15 μL water and 15 μL methanol/acetonitrile (1:1 v/v) (LC-MS optima grade, Thermo Fisher Scientific). Samples were centrifuged at 20,000 × *g* for 10 min at 4°C and the supernatants were transferred to Liquid Chromatography (LC) vials. The injection volume for polar metabolite analysis was 8 μl.

For metabolite abundances in Figure S4 a slightly modified protocol was used, as follows. The cell extracts were dissolved in 50 μL water (LC-MS optima grade, Thermo Fisher Scientific) and sonicated to ensure analytes were completely dissolved. Samples were centrifuged at 18,000 × *g* for 30 min at 4°C and the supernatants were transferred to Liquid Chromatography (LC) vials. The injection volume for polar metabolite analysis was 1 μl.

**[U-$^{13}$]-Glutamine Labeling—**Cells were grown to 80% confluence in 6-well plates with standard culture medium and washed with sterile PBS. Then, culture medium in which glutamine was replaced by [$^{13}C_5$]-L-glutamine (Cambridge Isotope Laboratories), supplemented with dialyzed FBS (GIBCO) and appropriate concentrations of inhibitors was added (1.5 ml/well). At the appropriate time-point, metabolites were extracted as described above.

**Liquid Chromatography—**A hydrophilic interaction liquid chromatography method (HILIC) with an Xbridge amide column (100 × 2.1 mm, 3.5 μm) (Waters) was employed on a Dionex (Ultimate 3000 UHPLC) for compound separation and detection at room temperature. The mobile phase A was 20 mM ammonium acetate and 15 mM ammonium hydroxide in water with 3% acetonitrile, pH 9.0, and the mobile phase B was acetonitrile. The linear gradient was as follows: 0 min, 85% B; 1.5 min, 85% B, 5.5 min, 35% B; 10 min, 35% B, 10.5 min, 35% B, 14.5 min, 35% B, 15 min, 85% B, and 20 min, 85% B. The flow rate was 0.15 ml/min from 0 to 10 min and 15 to 20 min, and 0.3 ml/min from 10.5 to 14.5 min. All solvents were LCMS grade and purchased from Thermo Fisher Scientific.

For metabolite abundances in Figure S4 a slightly modified protocol was used, as follows. A hydrophilic interaction liquid chromatography method (HILIC) with an ZORBAX HILIC Plus column (150 × 2.1 mm, 1.8 μm) (Agilent) was employed on a Dionex (Ultimate 3000

UHPLC) for compound separation and detection at room temperature. The mobile phase Water with 0.1% formic acid was mobile phase A and acetonitrile with 0.1% formic acid was mobile phase B. The linear gradient was as follows: 0 min, 95% B; 1.5 min, 95% B, 15.5 min, 50% B; 16.5 min, 10% B, 18.5 min, 10% B, 18.6 min, 95% B, 21 min, 95% B, and total flow rate was 0.5 ml/min. All solvents were LCMS grade and purchased from Thermo Fisher Scientific.

**Mass Spectrometry—**The Q Exactive MS (Thermo Scientific) is equipped with a heated electrospray ionization probe (HESI), and the relevant parameters are as listed: evaporation temperature, 120°C; sheath gas, 30; auxiliary gas, 10; sweep gas, 3; spray voltage, 3.6 kV for positive mode and 2.5 kV for negative mode. Capillary temperature was set at 320°C, and S-lens was 55. A full scan range from 60 to 900 (m/z) was used. The resolution was set at 70,000. The maximum injection time was 200 ms. Automated gain control (AGC) was targeted at 3,000,000 ions.

For metabolite abundances in Figure S4 a slightly modified protocol was used, as follows. The Q Exactive HF (Thermo Scientific) is equipped with a heated electrospray ionization probe (HESI), and the relevant parameters are as listed: evaporation temperature, 120°C; sheath gas, 60; auxiliary gas, 20; sweep gas, 1; spray voltage, 3.0 kV for negative mode. Capillary temperature was set at 380°C, and S-lens was 50. A full scan range from 80 to 300 (m/z) was used. The resolution was set at 240,000. The maximum injection time was 500 ms. Automated gain control (AGC) was targeted at 3,000,000 ions.

**Metabolomics and Data Analysis—**Raw data collected from LC-Q Exactive MS were processed on Sieve 2.0 (Thermo Scientific) and ToxID 2.0 (Thermo Scientific). Peak alignment and detection were performed according to the protocol described by Thermo Scientific. For targeted metabolite analysis, the method ‘peak alignment and frame extraction’ was applied. An input file of theoretical m/z and detected retention time of 204 known metabolites was used for targeted metabolites analysis with data collected in positive mode, while a separate input file of 278 metabolites was used for negative mode. M/Z width was set at 10 ppm. The output file including detected m/z and relative intensity in different samples was obtained after data processing. The quantity of the metabolite fraction analyzed was adjusted to the corresponding protein concentration and cell count upon processing a parallel 6-well plate. Quantitation and statistics were calculated and visualized with Microsoft Excel, MORPHEUS and MetaboAnalyst online software.

## QUANTIFICATION AND STATISTICAL ANALYSIS

Data are shown as mean ± standard deviation (SD) or mean ± standard error of the mean (SEM), and the number of replicates is indicated in the figure legends. Statistical significance was determined using a two-tailed Student’s t-test. Significance: *$p \leq 0.05$, **$p \leq 0.01$.

## DATA AND CODE AVAILABILITY

This manuscript did not generate new datasets or code.

## Supplementary Material

Refer to Web version on PubMed Central for supplementary material.

## ACKNOWLEDGMENTS

The authors thank Cindy Westmiller for assisting with manuscript preparation. M.J.L. gratefully acknowledges a postdoctoral research award from the Breast Cancer Coalition of Rochester. A.A.C. gratefully acknowledges a graduate fellowship from the King Abdullah International Medical Research Center under the Ministry of National Guard Health Affairs, Saudi Arabia. The authors would like to thank Dr. Patrick Stover and Olga Malysheva for access to the LC-HRMS instrumentation, and Dr. Hening Lin and Dr. Sushabhan Sadhukhan for providing HPLC columns and initial technical advice. The authors would also like to thank Cerione lab members for the critical reading of this manuscript, helpful comments, and discussion. This work was supported by NIH grants GM122575 and CA201402 to R.A.C.

## REFERENCES

Altman BJ, Stine ZE, and Dang CV (2016). From Krebs to clinic: glutamine metabolism to cancer therapy. Nat. Rev. Cancer 16, 619–634. [PubMed: 27492215]

Asselin-Labat ML, Sutherland KD, Barker H, Thomas R, Shackleton M, Forrest NC, Hartley L, Robb L, Grosveld FG, van der Wees J, et al. (2007). Gata-3 is an essential regulator of mammary-gland morphogenesis and luminal-cell differentiation. Nat. Cell Biol 9, 201–209. [PubMed: 17187062]

Biancur DE, Paulo JA, Ma1achowska B, Quiles Del Rey M, Sousa CM, Wang X, Sohn ASW, Chu GC, Gygi SP, Harper JW, et al. (2017). Compensatory metabolic networks in pancreatic cancers upon perturbation of glutamine metabolism. Nat. Commun 8, 15965. [PubMed: 28671190]

Cardona C, Sánchez-Mejías E, Dávila JC, Martín-Rufián M, Campos-Sandoval JA, Vitorica J, Alonso FJ, Matés JM, Segura JA, Norenberg MD, et al. (2015). Expression of Gls and Gls2 glutaminase isoforms in astrocytes. Glia 63, 365–382. [PubMed: 25297978]

Cluntun AA, Huang H, Dai L, Liu X, Zhao Y, and Locasale JW (2015). The rate of glycolysis quantitatively mediates specific histone acetylation sites. Cancer Metab 3, 10. [PubMed: 26401273]

Cluntun AA, Lukey MJ, Cerione RA, and Locasale JW (2017). Glutamine metabolism in cancer: understanding the heterogeneity. Trends Cancer 3, 169–180. [PubMed: 28393116]

Dai X, Li T, Bai Z, Yang Y, Liu X, Zhan J, and Shi B (2015). Breast cancer intrinsic subtype classification, clinical use and future trends. Am. J. Cancer Res 5, 2929–2943. [PubMed: 26693050]

Farré D, Roset R, Huerta M, Adsuara JE, Roselló L, Albà MM, and Messeguer X (2003). Identification of patterns in biological sequences at the ALGGEN server: PROMO and MALGEN. Nucleic Acids Res 31, 3651–3653. [PubMed: 12824386]

Gao P, Tchernyshyov I, Chang T-C, Lee Y-S, Kita K, Ochi T, Zeller KI, De Marzo AM, Van Eyk JE, Mendell JT, and Dang CV (2009). c-Myc suppression of miR-23a/b enhances mitochondrial glutaminase expression and glutamine metabolism. Nature 458, 762–765. [PubMed: 19219026]

Gross MI, Demo SD, Dennison JB, Chen L, Chernov-Rogan T, Goyal B, Janes JR, Laidig GJ, Lewis ER, Li J, et al. (2014). Antitumor activity of the glutaminase inhibitor CB-839 in triple-negative breast cancer. Mol. Cancer Ther 13, 890–901. [PubMed: 24523301]

Hu W, Zhang C, Wu R, Sun Y, Levine A, and Feng Z (2010). Glutaminase 2, a novel p53 target gene regulating energy metabolism and antioxidant function. Proc. Natl. Acad. Sci. USA 107, 7455–7460. [PubMed: 20378837]

Huang Q, Stalnecker C, Zhang C, McDermott LA, Iyer P, O'Neill J, Reimer S, Cerione RA, and Katt WP (2018). Characterization of the interactions of potent allosteric inhibitors with glutaminase C, a key enzyme in cancer cell glutamine metabolism. J. Biol. Chem 293, 3535–3545. [PubMed: 29317493]

Hutson SM, Williams GD, Berkich DA, LaNoue KF, and Briggs RW (1992). A $^{31}$P NMR study of mitochondrial inorganic phosphate visibility: effects of $Ca^{2+}$, $Mn^{2+}$, and the pH gradient. Biochemistry 31, 1322–1330. [PubMed: 1736991]

Katt WP, Ramachandran S, Erickson JW, and Cerione RA (2012). Dibenzophenanthridines as inhibitors of glutaminase C and cancer cell proliferation. Mol. Cancer Ther 11, 1269–1278. [PubMed: 22496480]

Katt WP, Lukey MJ, and Cerione RA (2017). A tale of two glutaminases: homologous enzymes with distinct roles in tumorigenesis. Future Med. Chem 9, 223–243. [PubMed: 28111979]

Koboldt DC, Fulton RS, McLellan MD, Schmidt H, Kalicki-Veizer J, McMichael JF, Fulton LL, Dooling DJ, Ding L, Mardis ER, et al.; Cancer Genome Atlas Network (2012). Comprehensive molecular portraits of human breast tumours. Nature 490, 61–70. [PubMed: 23000897]

Lacey JH, Bradford NM, Joseph SK, and McGivan JD (1981). Increased activity of phosphate-dependent glutaminase in liver mitochondria as a result of glucagon treatment of rats. Biochem. J 194, 29–33. [PubMed: 7305982]

Liu X, Ser Z, Cluntun AA, Mentch SJ, and Locasale JW (2014). A strategy for sensitive, large scale quantitative metabolomics. J. Vis. Exp 2014, 51358.

Lukey MJ, Greene KS, Erickson JW, Wilson KF, and Cerione RA (2016). The oncogenic transcription factor c-Jun regulates glutaminase expression and sensitizes cells to glutaminase-targeted therapy. Nat. Commun 7, 11321. [PubMed: 27089238]

Matés JM, Campos-Sandoval JA, and Márquez J (2018). Glutaminase isoenzymes in the metabolic therapy of cancer. Biochim Biophys Acta Rev Cancer 1870, 158–164. [PubMed: 30053497]

Messeguer X, Escudero R, Farré D, Núñez O, Martínez J, and Albà MM (2002). PROMO: detection of known transcription regulatory elements using species-tailored searches. Bioinformatics 18, 333–334. [PubMed: 11847087]

Miller RA, Shi Y, Lu W, Pirman DA, Jatkar A, Blatnik M, Wu H, Cárdenas C, Wan M, Foskett JK, et al. (2018). Targeting hepatic glutaminase activity to ameliorate hyperglycemia. Nat. Med 24, 518–524. [PubMed: 29578539]

Muir A, Danai LV, Gui DY, Waingarten CY, Lewis CA, and Vander Heiden MG (2017). Environmental cystine drives glutamine anaplerosis and sensitizes cancer cells to glutaminase inhibition. eLife 6, e27713. [PubMed: 28826492]

Pavlova NN, and Thompson CB (2016). The emerging hallmarks of cancer metabolism. Cell Metab 23, 27–47. [PubMed: 26771115]

Possemato R, Marks KM, Shaul YD, Pacold ME, Kim D, Birsoy K, Sethumadhavan S, Woo H-K, Jang HG, Jha AK, et al. (2011). Functional genomics reveal that the serine synthesis pathway is essential in breast cancer. Nature 476, 346–350. [PubMed: 21760589]

Rauch U, Schulze K, Witzenbichler B, and Schultheiss HP (1994). Alteration of the cytosolic-mitochondrial distribution of high-energy phosphates during global myocardial ischemia may contribute to early contractile failure. Circ. Res 75, 760–769. [PubMed: 7923621]

Robinson MM, McBryant SJ, Tsukamoto T, Rojas C, Ferraris DV, Hamilton SK, Hansen JC, and Curthoys NP (2007). Novel mechanism of inhibition of rat kidney-type glutaminase by bis-2-(5-phenylacetamido-1,2,4-thiadiazol-2-yl)ethyl sulfide (BPTES). Biochem. J 406, 407–414. [PubMed: 17581113]

Shin CS, Mishra P, Watrous JD, Carelli V, D'Aurelio M, Jain M, and Chan DC (2017). The glutamate/cystine xCT antiporter antagonizes glutamine metabolism and reduces nutrient flexibility. Nat. Commun 8, 15074. [PubMed: 28429737]

Stalnecker CA, Ulrich SM, Li Y, Ramachandran S, McBrayer MK, De-Berardinis RJ, Cerione RA, and Erickson JW (2015). Mechanism by which a recently discovered allosteric inhibitor blocks glutamine metabolism in transformed cells. Proc. Natl. Acad. Sci. USA 112, 394–399. [PubMed: 25548170]

Suzuki S, Tanaka T, Poyurovsky MV, Nagano H, Mayama T, Ohkubo S, Lokshin M, Hosokawa H, Nakayama T, Suzuki Y, et al. (2010). Phosphate-activated glutaminase (GLS2), a p53-inducible regulator of glutamine metabolism and reactive oxygen species. Proc. Natl. Acad. Sci. USA 107, 7461–7466. [PubMed: 20351271]

Tomayko MM, and Reynolds CP (1989). Determination of subcutaneous tumor size in athymic (nude) mice. Cancer Chemother. Pharmacol 24, 148–154. [PubMed: 2544306]

van Geldermalsen M, Wang Q, Nagarajah R, Marshall AD, Thoeng A, Gao D, Ritchie W, Feng Y, Bailey CG, Deng N, et al. (2016). ASCT2/ SLC1A5 controls glutamine uptake and tumour growth in triple-negative basal-like breast cancer. Oncogene 35, 3201–3208. [PubMed: 26455325]

Vander Heiden MG, and DeBerardinis RJ (2017). Understanding the intersections between metabolism and cancer biology. Cell 168, 657–669. [PubMed: 28187287]

Wang JB, Erickson JW, Fuji R, Ramachandran S, Gao P, Dinavahi R, Wilson KF, Ambrosio AL, Dias SM, Dang CV, and Cerione RA (2010). Targeting mitochondrial glutaminase activity inhibits oncogenic transformation. Cancer Cell 18, 207–219. [PubMed: 20832749]

Watford M (1993). Hepatic glutaminase expression: relationship to kidney-type glutaminase and to the urea cycle. FASEB J 7, 1468–1474. [PubMed: 8262331]

Watford M, and Smith EM (1990). Distribution of hepatic glutaminase activity and mRNA in perivenous and periportal rat hepatocytes. Biochem. J 267, 265–267. [PubMed: 1970242]

Wu C, Chen L, Jin S, and Li H (2018). Glutaminase inhibitors: a patent review. Expert Opin. Ther. Pat 28, 823–835. [PubMed: 30273516]

Xiao D, Ren P, Su H, Yue M, Xiu R, Hu Y, Liu H, and Qing G (2015). Myc promotes glutaminolysis in human neuroblastoma through direct activation of glutaminase 2. Oncotarget 6, 40655–40666. [PubMed: 26528759]

Zhang C, Liu J, Zhao Y, Yue X, Zhu Y, Wang X, Wu H, Blanco F, Li S, Bhanot G, et al. (2016). Glutaminase 2 is a novel negative regulator of small GTPase Rac1 and mediates p53 function in suppressing metastasis. eLife 5, e10727. [PubMed: 26751560]

## Highlights

- Basal- and luminal-subtype breast cancers express GLS and GLS2, respectively
- GLS2 expression in breast cancer is regulated by promoter methylation and GATA3
- GLS2 supports proliferation and tumorigenesis in luminal-subtype breast cancers
- 968 inhibits GLS2 to suppress luminal-subtype breast cancer growth

## SIGNIFICANCE

Humans have two genes encoding glutaminase enzymes, *GLS* and *GLS2*. Efforts to target glutamine catabolism for cancer therapy have focused on GLS, an inhibitor of which (CB-839) is currently in clinical trials. The GLS2 isozyme has previously been described as a tumor suppressor, with downregulated expression in liver cancer. We report here that GLS2 is overexpressed and essential for growth in the most prevalent subtypes of breast cancer, luminal A and B. Although GLS2 is insensitive to CB-839-class drugs, it is inhibited by the small molecule 968, which suppresses breast tumor growth *in vivo*. These findings establish a critical role for GLS2 in breast cancer and advance our understanding of how to target aberrant glutamine metabolism for cancer therapy.

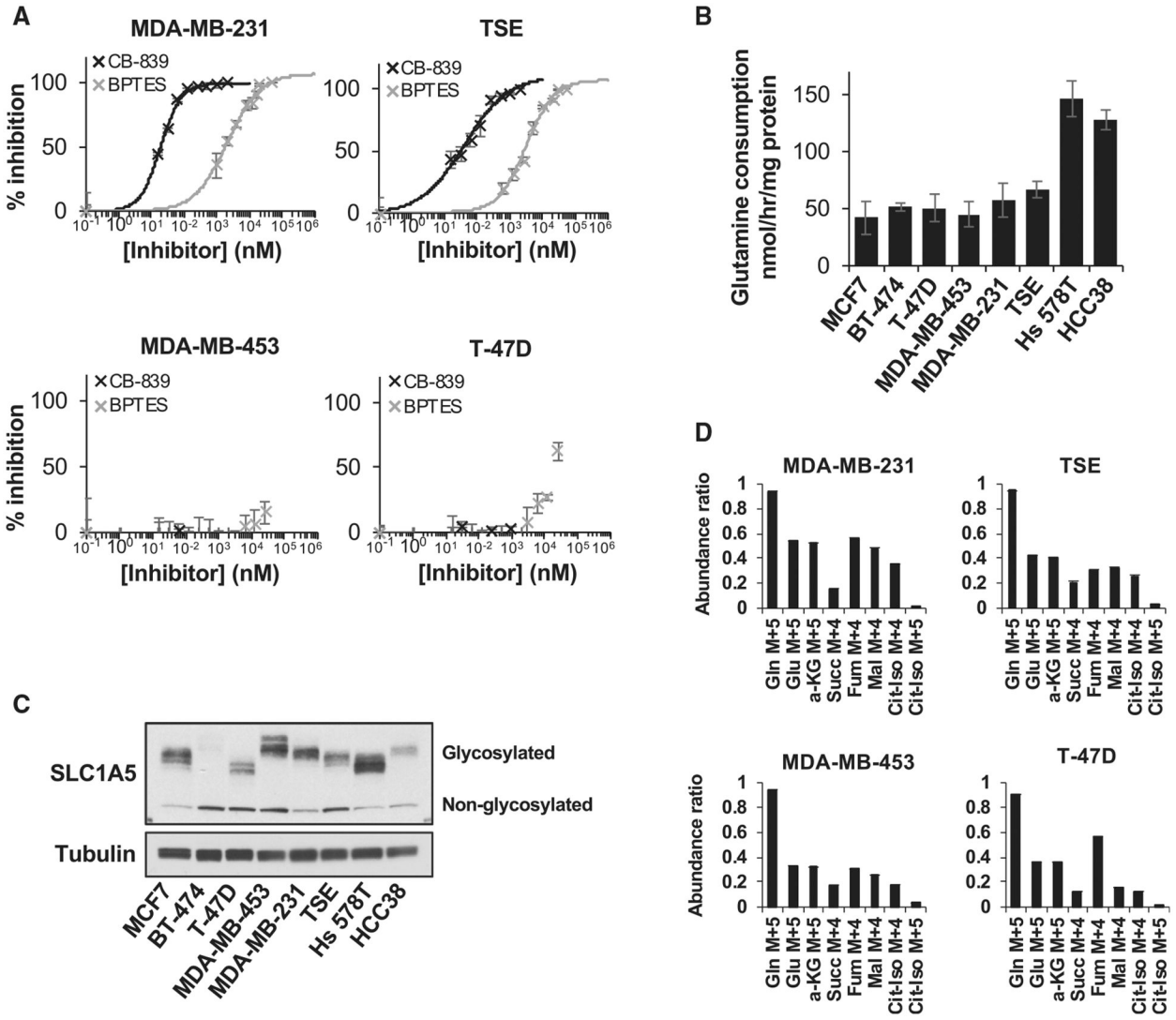


**Figure 1. Luminal-Subtype Breast Cancer Cells Use Glutamine to Supply the TCA Cycle, but Resist GLS Inhibitors**

(A) The effect of the GLS inhibitors BPTES and CB-839 on proliferation of basal-subtype (MDA-MB-231 and TSE) and luminal-subtype (MDA-MB-453 and T-47D) breast cancer cells over 6 days. Mean ± SD of triplicate assays.

(B) Glutamine consumption rates, per milligram of total cellular protein, of breast cancer cell lines. Mean ± SD of biological triplicates.

(C) Western blot showing relative levels of SLC1A5 in breast cancer cell lines. Note that SLC1A5 is an integral membrane protein subject to covalent posttranslational modifications including glycosylations, which cause it to run at a range of molecular weights on SDS-PAGE.

(D) Abundance ratios of fully labeled intracellular glutamine, glutamate, and TCA cycle metabolites in breast cancer cells supplied with [U-$^{13}$C]-glutamine for 10 h. Mean ± SEM of biological triplicate samples.

See also Figure S1 and Tables S1–S3.

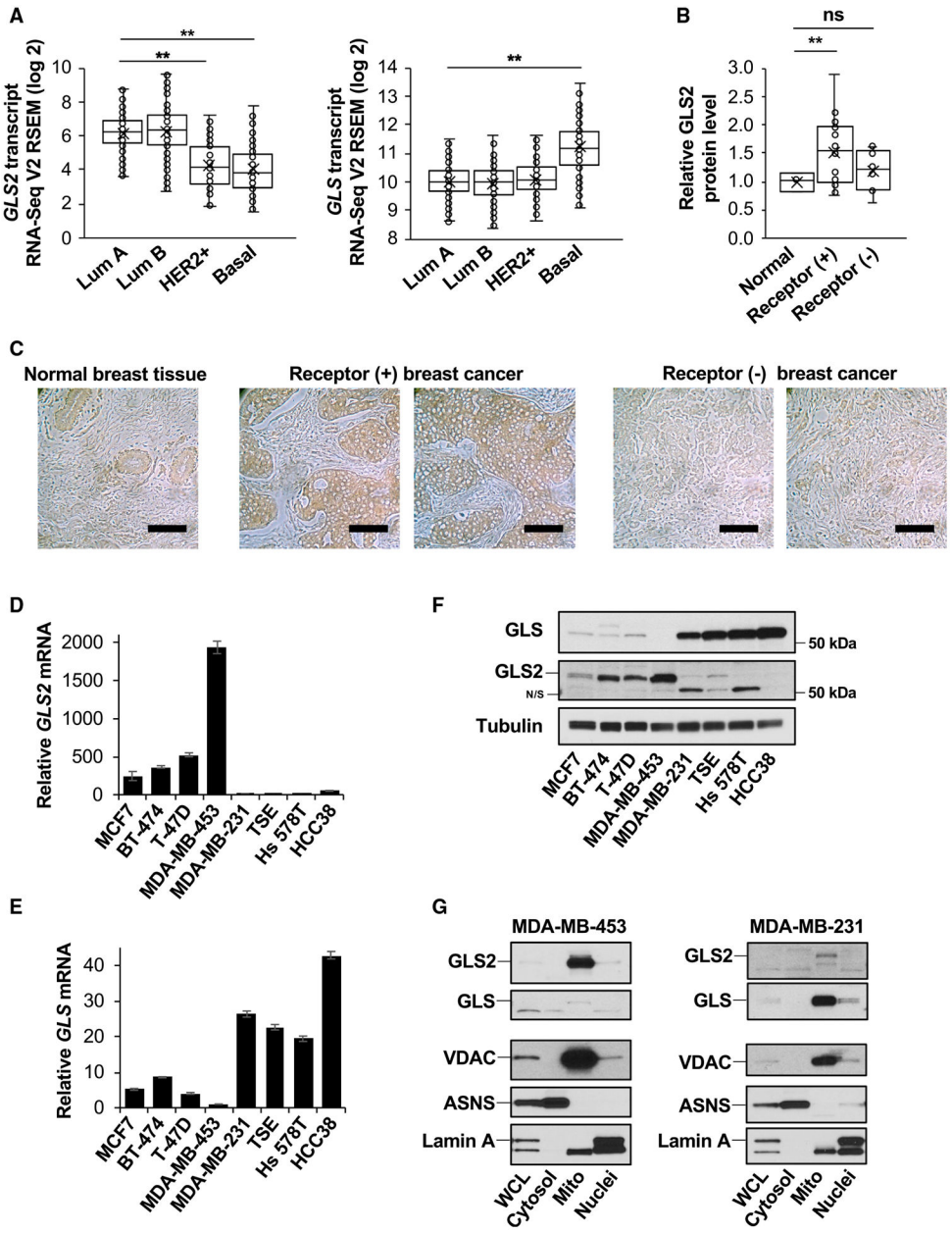


**Figure 2. GLS2 Is Upregulated in Luminal-Subtype Breast Cancers**

(A) Box and whisker plots showing transcript levels of *GLS2* (left panel) and *GLS* (right panel) in the molecular subtypes of breast cancer. RNA-seq V2 RSEM data are from The Cancer Genome Atlas invasive breast cancer dataset. The mean expression in each group is indicated by a cross, and the box and whiskers indicate the minimum, first quartile, median, third quartile, and maximum values. **$p \leq 0.01$.

(B) Relative GLS2 protein levels in tissue microarray slices of normal mammary tissue, receptor-positive, and receptor-negative breast tumors. **$p \leq 0.01$.

(C) Microscopy images of breast tissue microarray slices stained brown for GLS2. Representative images are shown for normal breast tissue along with receptor-positive and receptor-negative breast tumors. Scale bars, 200 μm.

(D) Quantitative real-time PCR data showing relative levels of *GLS2* transcript in breast cancer cell lines. Reactions were carried out in triplicate, and error bars indicate the $RQ_{max}$ and $RQ_{min}$ values.
(E) Quantitative real-time PCR data showing relative levels of *GLS* transcript in breast cancer cell lines. Reactions were carried out in triplicate, and error bars indicate the $RQ_{max}$ and $RQ_{min}$ values.
(F) Western blots showing relative levels of GLS and GLS2 in breast cancer cell lines. A non-specific band from the GLS2 antibody, clearly visible for MDA-MB-231 and Hs 578T lysates, is labeled N/S.
(G) Western blots of whole-cell lysates (WCLs), and cytosolic, mitochondrial, and nuclear fractions from MDA-MB-453 and MDA-MB-231 cells. VDAC, ASNS, and Lamin A serve as mitochondrial, cytosolic, and nuclear marker proteins, respectively.
See also Figure S2.

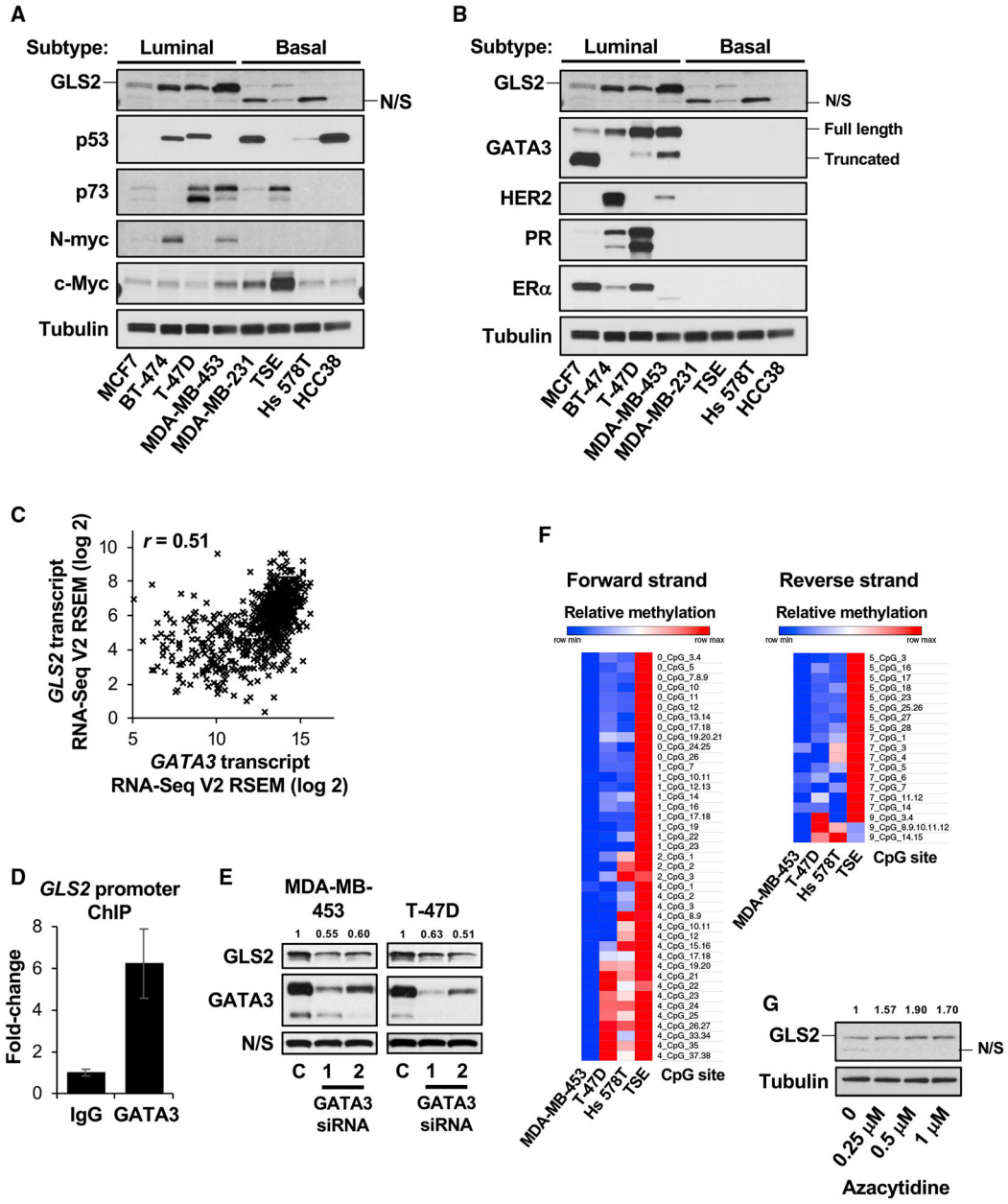


**Figure 3. *GLS2* Gene Expression Is Regulated by GATA3 and Promoter Methylation**

(A) Western blots showing relative levels of GLS2, and previously identified transcription factors for the *GLS2* gene, in breast cancer cell lines.

(B) Western blots showing relative levels of GLS2, the luminal-transcription factor GATA3, and the receptors ERα, PR, and HER2 in breast cancer cell lines.

(C) Plot of *GLS2* and *GATA3* transcript levels in human breast tumors, with the Pearson correlation coefficient r indicated. RNA-seq V2 RSEM data from TCGA invasive breast cancer dataset.

(D) Quantitative real-time PCR data showing relative levels of a 176-bp fragment of the *GLS2* gene promoter, centered on the putative GATA3 binding site, in chromatin

immunoprecipitations (ChIPs) using negative control IgG or a GATA3-targeted antibody. Mean ± SD of biological triplicate samples.

(E) Western blots showing GLS2 and GATA3 levels in MDA-MB-453 and T-47D cells transfected with either a control siRNA (labeled C) or with two independent GATA3-targeted siRNAs. Bands in the GLS2 blot were quantified by densitometry using ImageJ, and relative band intensities are indicated above the blot. Since GATA3 regulates expression of Tubulin and several other cytoskeletal proteins, a non-specific (N/S) band is shown to demonstrate equal loading.

(F) Heatmaps showing relative methylation levels at CpG sites within the CpG island of the *GLS2* gene promoter in breast cancer cell lines. Labels for the CpG sites refer to the amplicon in which the sites are located (amplicons 0 to 9) and then the position of the site within that amplicon (i.e., first CpG site, second CpG site, etc.). Numbers missing in the sequence are for sites at which methylation ratios could not be determined. Although the amplicons were designed to overlap, only a single reading is shown for sites covered by more than one amplicon.

(G) Western blot showing relative levels of GLS2 in TSE cells treated with different concentrations of the DNA hypomethylating agent azacitidine for 48 h. Bands in the GLS2 blot were quantified by densitometry using ImageJ, and relative band intensities are indicated above the blot. A non-specific band is labeled N/S. See also Figure S3.

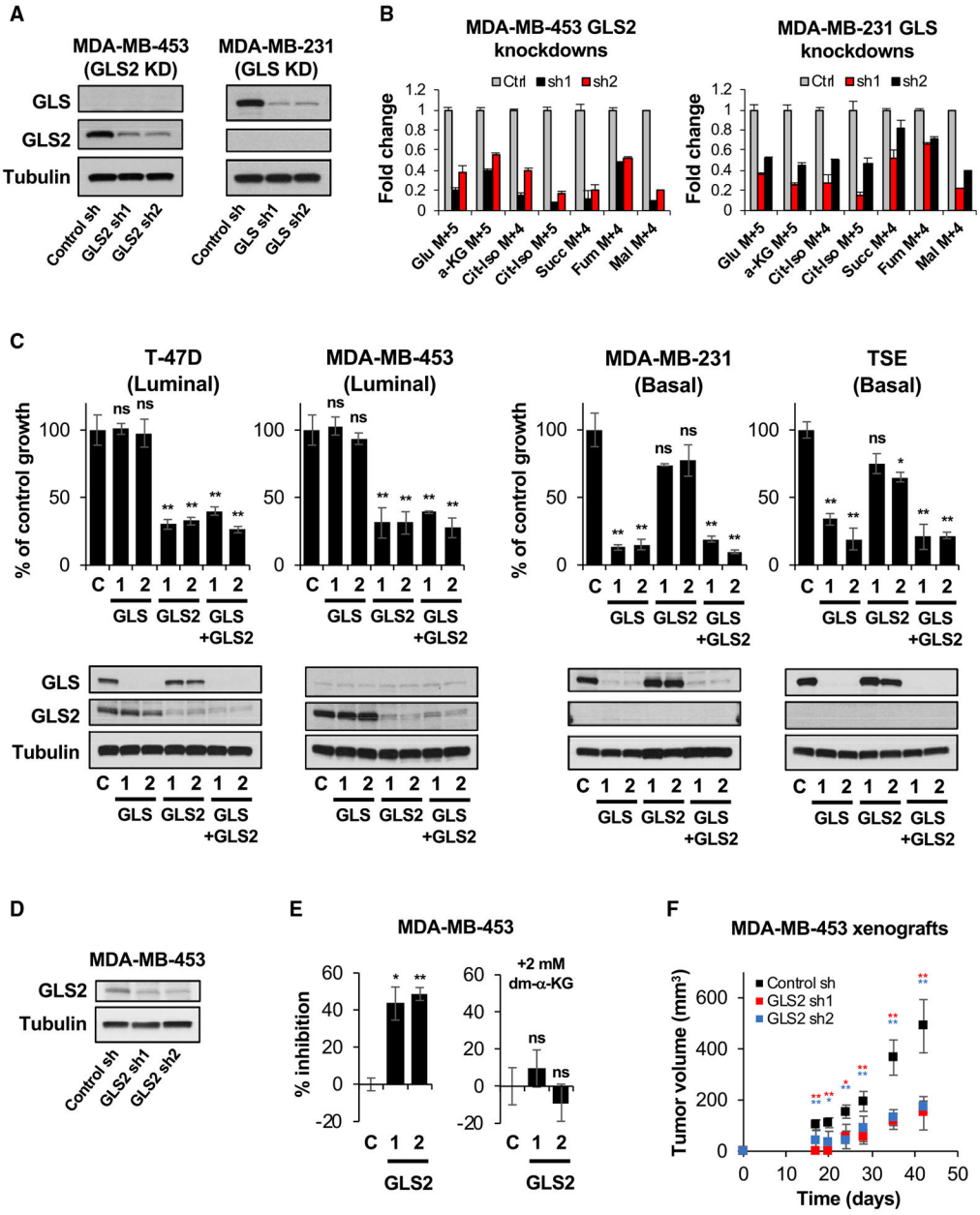


**Figure 4. GLS2 Is Essential in Luminal-Subtype Breast Cancers**

(A) Western blots showing GLS and GLS2 levels in MDA-MB-453 cells and MDA-MB-231 cells expressing either a control shRNA or two independent GLS2-targeted (MDA-MB-453 cells) or GLS-targeted (MDA-MB-231 cells) shRNAs.

(B) Fold changes in fully labeled glutamate and TCA cycle metabolites (i.e., derived directly from [U-$^{13}$C]-glutamine) in MDA-MB-453 cells following knockdown of GLS2, or in MDA-MB-231 cells following knockdown of GLS. Mean ± SEM of biological triplicates.

(C) The effect of knocking down either GLS, GLS2, or both GLS and GLS2 simultaneously, on the proliferation of breast cancer cell lines over 6 days. For each condition, two independent siRNAs were used, and the effects were compared with those of a control

siRNA (labeled C). Mean ± SD of triplicate assays. Lower panels show western blots for GLS and GLS2 in each sample. *p ≤ 0.05; **p ≤ 0.01; ns, not significant.

(D) Western blot showing partial knockdown of GLS2 in MDA-MB-453 stably expressing two independent GLS2-targeted shRNAs, relative to cells stably expressing a control shRNA.

(E) Inhibition of proliferation over 6 days for MDA-MB-453 cells stably expressing GLS2-targeted shRNAs, relative to cells stably expressing a control shRNA (labeled C). Experiments were run either without (left panel) or with (right panel) supplementation of the culture medium with 2 mM dimethyl α-ketoglutarate (dm-α-KG). Mean ± SD of triplicate assays. *p ≤ 0.05; **p ≤ 0.01; ns, not significant.

(F) Growth of xenograft tumors in mice by MDA-MB-453 cells stably expressing either a control shRNA or two independent GLS2-targeted shRNAs. Mean ± SD (n = 6 tumors per condition). *p ≤ 0.05; **p ≤ 0.01.

See also Figure S4.

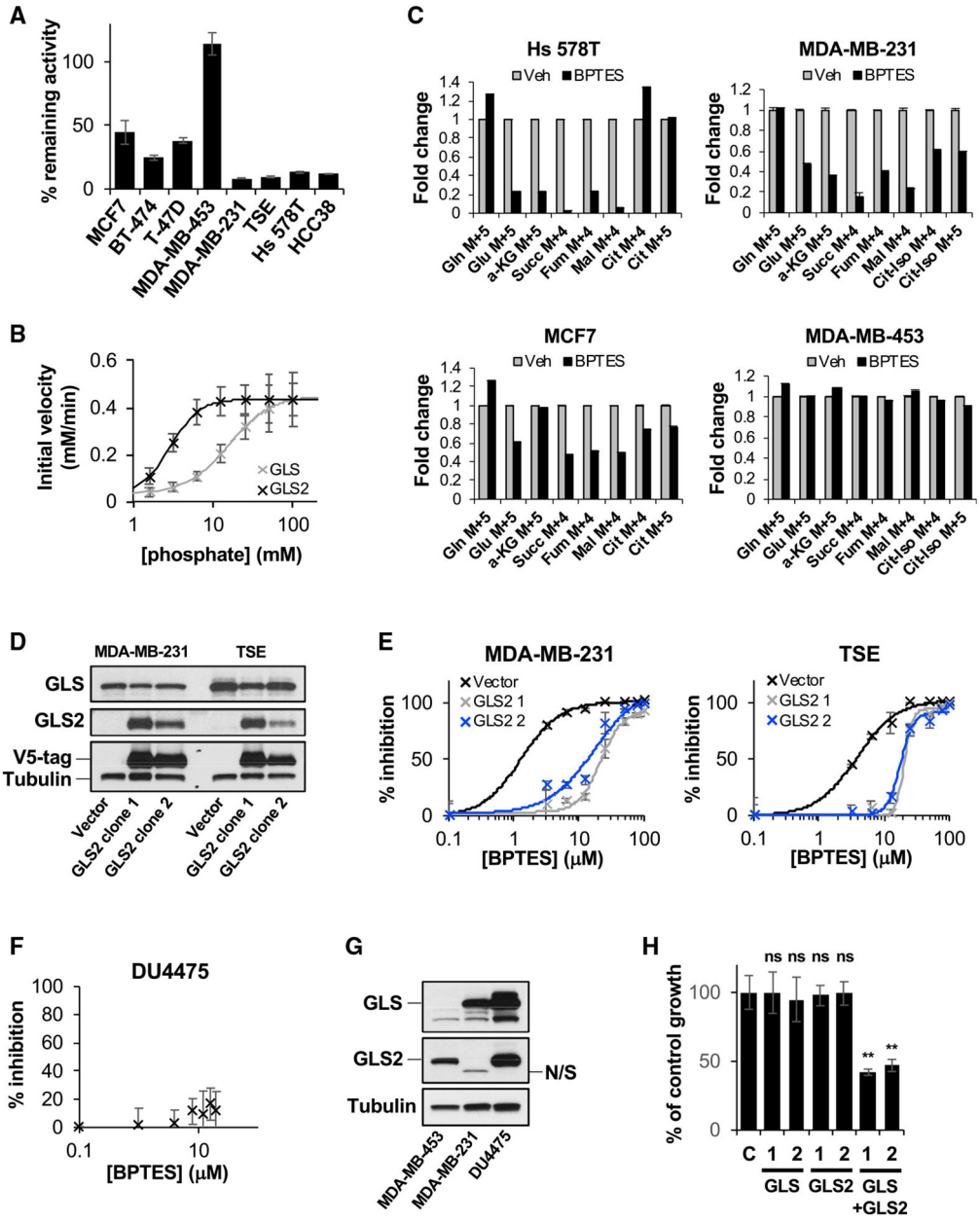


**Figure 5. GLS2 Expression Is Sufficient for Resistance to GLS Inhibitors**

(A) Inhibition of glutaminase activity by 10 μM BPTES in mitochondria isolated from breast cancer cell lines. Plot shows activity in the presence of 10 μM BPTES relative to matched samples with no BPTES present. Mean ± SD of triplicate assays.

(B) The effect of increasing inorganic phosphate concentrations on the catalytic activity of recombinant full-length human GLS (GAC splice variant) and GLS2. Mean ± SD of triplicate assays.

(C) Fold changes in fully labeled intracellular metabolites (i.e., derived directly from [U-$^{13}$C]-glutamine) in basal-subtype (top) and luminal-subtype (bottom) breast cancer cell lines, following treatment with 10 μM BPTES. Mean ± SEM of triplicates relative to the vehicle.

(D) Western blots showing levels of endogenous GLS and ectopically expressed V5-tagged GLS2 in MDA-MB-231 and TSE cells.
(E) Inhibition of proliferation over 6 days of MDA-MB-231 and TSE cells, stably expressing GLS2 (two clones for each cell line) or carrying the plasmid vector only, by treatment with different concentrations of BPTES. Mean ± SD of triplicate assays.
(F) The effect of different concentrations of BPTES on proliferation of DU4475 cells over 6 days. Mean ± SD of triplicate assays.
(G) Western blots showing relative levels of GLS and GLS2 in MDA-MB-453, MDA-MB-231, and DU4475 cells. A non-specific band from the GLS antibody is marked N/S.
(H) The effect of knocking down either GLS or GLS2, or both GLS and GLS2 simultaneously, on the proliferation of DU4475 cells over 6 days. For each condition, two independent siRNAs were used, and the effects were compared with those of a control siRNA (labeled C). Mean ± SD of triplicate assays. **$p \leq 0.01$; ns, not significant.
See also Figure S5 and Table S4.

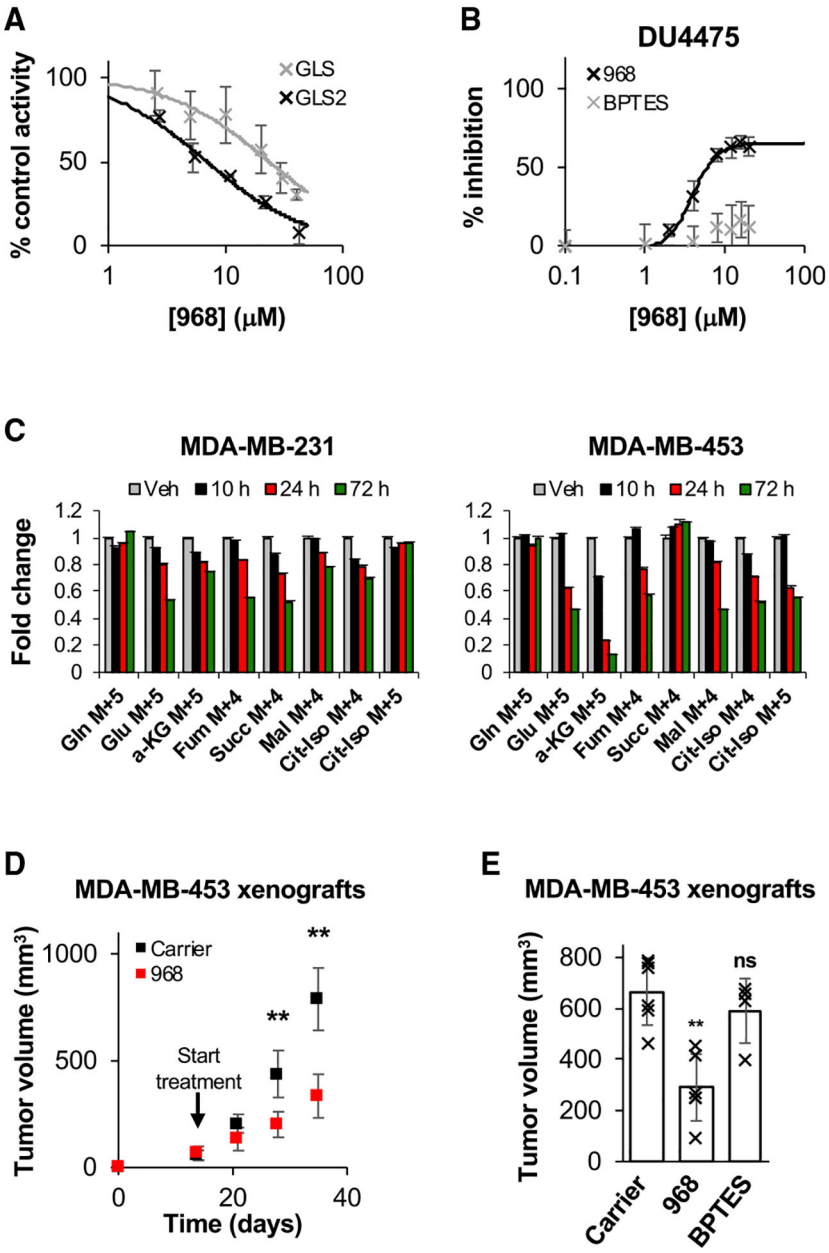


**Figure 6. 968 Inhibits GLS2 and Suppresses BPTES-Resistant Breast Cancer Growth**

(A) Inhibition of purified recombinant full-length human GLS (GAC splice variant) or GLS2 by different concentrations of 968. Mean ± SD of triplicate assays.

(B) The effect of different concentrations of 968 or BPTES on proliferation of DU4475 cells over 6 days. Mean ± SD of triplicate assays.

(C) Fold changes in fully labeled intracellular metabolites, derived directly from [U-$^{13}$C]-glutamine, when breast cancer cells are treated with 10 μM 968 for the indicated periods of time. Mean ± SEM of triplicates relative to the vehicle.

(D) Growth of MDA-MB-453 xenograft tumors in mice. Once palpable tumors were detected (at day 14), mice were divided into two groups, one of which received

subcutaneous injections of 10 mg/kg 968 three times per week, while the other received carrier solution only. Mean ± SD (n = 6 tumors per condition). **p ≤ 0.01.
(E) Plot showing the final size of MDA-MB-453 xenograft tumors following treatment of mice with 10 mg/kg 968, 10 mg/kg BPTES, or carrier solution only, three times per week from day 14 until day 35. Mice were sacrificed at day 35, and tumors were excised prior to measurement. Mean ± SD (n = 6 tumors per condition). **p ≤ 0.01; ns, not significant.
See also Figure S6 and Table S4.

## KEY RESOURCES TABLE

| REAGENT or RESOURCE | SOURCE | IDENTIFIER |
|---|---|---|
| Antibodies | | |
| ASCT2 Antibody | Cell Signaling Technology | Cat# 5345; RRID:AB_10621427 |
| α/β-Tubulin Antibody | Cell Signaling Technology | Cat# 2148; RRID:AB_2288042 |
| GLS2 antibody (C-term E513) | Abgent | Cat# AP6650D; RRID:AB_10818414 |
| GLS antibody (C-term) | Abgent | Cat# AP8809b; RRID:AB_10553123 |
| Anti-GLS2 antibody | Abcam | Cat# ab150474 |
| 4F2hc/CD98 Rabbit mAb | Cell Signaling Technology | Cat# 13180; RRID:AB_2687475 |
| xCT/SLC7A11 Rabbit mAb | Cell Signaling Technology | Cat# 12691; RRID:AB_2687474 |
| VDAC Rabbit mAb | Cell Signaling Technology | Cat# 4661; RRID:AB_10557420 |
| ASNS Antibody | Proteintech | Cat# 14681–1-AP; RRID:AB_2060119 |
| Lamin A/C Mouse mAb | Cell Signaling Technology | Cat# 4777; RRID:AB_10545756 |
| p53 Mouse mAb | Cell Signaling Technology | Cat# 2524; RRID:AB_331743 |
| p63 Rabbit mAb | Cell Signaling Technology | Cat# 39692; RRID:AB_2799159 |
| p73 Rabbit mAb | Cell Signaling Technology | Cat# 14620; RRID:AB_2798542 |
| N-Myc Rabbit mAb | Cell Signaling Technology | Cat# 51705; RRID:AB_2799400 |
| c-Myc Rabbit mAb | Cell Signaling Technology | Cat# 5605; RRID:AB_1903938 |
| GATA-3 Rabbit mAb | Cell Signaling Technology | Cat# 5852; RRID:AB_10835690 |
| HER2/ErbB2 Rabbit mAb | Cell Signaling Technology | Cat# 4290; RRID:AB_10828932 |
| Progesterone Receptor A/B Rabbit mAb | Cell Signaling Technology | Cat# 8757; RRID:AB_2797144 |
| Estrogen Receptor α Rabbit mAb | Cell Signaling Technology | Cat# 13258; RRID:AB_2632959 |
| HSP60 Rabbit mAb | Cell Signaling Technology | Cat# 12165; RRID:AB_2636980 |
| HA-Tag Mouse mAb | Cell Signaling Technology | Cat# 2367; RRID:AB_10691311 |
| Myc-Tag Rabbit mAb | Cell Signaling Technology | Cat# 2278; RRID:AB_10693332 |
| V5 Tag Monoclonal Antibody | Thermo Fisher Scientific | Cat# R960–25; RRID:AB_2556564 |
| Anti-rabbit IgG, HRP-linked Antibody | Cell Signaling Technology | Cat# 7074; RRID:AB_2099233 |
| Anti-mouse IgG, HRP-linked Antibody | Cell Signaling Technology | Cat# 7076; RRID:AB_330924 |
| Bacterial and Virus Strains | | |
| *Escherichia coli* BL21(DE3) | Thermo Fisher Scientific | Cat# C600003 |
| Chemicals, Peptides, and Recombinant Proteins | | |
| Recombinant human Glutaminase C | This paper | N/A |
| Recombinant human GLS2 | This paper | N/A |
| SuperScript III Reverse Transcriptase | Thermo Fisher Scientific | Cat# 18080044 |
| RNase One Ribonuclease | Promega | Cat# M4261 |
| CB-839 | Millipore-Sigma | Cat#533717 |
| BPTES | Dr. Scott Ulrich, Ithaca College | N/A |
| 968 | ChemBridge Corporation | N/A |
| Dimethyl 2-oxoglutarate | Sigma-Aldrich | Cat# 349631 |
| [$^{13}C_5$]-L-Glutamine | Cambridge Isotope Laboratories | Item# CLM-1822-H-PK |
| Critical Commercial Assays | | |
| L-Glutamine/Ammonia Assay Kit (Rapid) | Megazyme | Cat# K-GLNAM |

| REAGENT or RESOURCE | SOURCE | IDENTIFIER |
|---|---|---|
| Protein Assay Dye Reagent Concentrate | Bio-Rad | Cat# 5000006 |
| Deposited Data | | |
| TCGA Breast Invasive Carcinoma (BRCA) gene expression RNaseq | The Cancer Genome Atlas, UCSC Xena, cBioPortal | https://xena.ucsc.edu, http://www.cbioportal.org |
| Human reference genome GRCh38/hg38 | UCSC Genome Browser, NCBI | https://genome.ucsc.edu, https://www.ncbi.nlm.nih.gov/gene/27165 |
| Experimental Models: Cell Lines | | |
| Human: MCF7 | ATCC | Cat# HTB-22 |
| Human: BT-474 | ATCC | Cat# HTB-20 |
| Human: T-47D | ATCC | Cat# HTB-133 |
| Human: MDA-MB-453 | ATCC | Cat# HTB-131 |
| Human: MDA-MB-231 | ATCC | Cat# HTB-26 |
| Human: TSE | Dr. Steven Abcouwer, University of Michigan | N/A |
| Human: Hs 578T | ATCC | Cat# HTB-126 |
| Human: HCC38 | ATCC | Cat# CRL-2314 |
| Human: SK-BR-3 | ATCC | Cat# HTB-30 |
| Human: DU4475 | ATCC | Cat# HTB-123 |
| Human: 293T | ATCC | Cat# CRL-3216 |
| Experimental Models: Organisms/Strains | | |
| Mouse: NOD.Cg-*Prkdc*$^{scid}$ *Il2rg*$^{tm1Wjl}$/SzJ (NSG), female, 6–8 weeks | The Jackson Laboratory | Stock# 005557 |
| Oligonucleotides | | |
| Primers | Table S6 | N/A |
| Silencer Select Negative Control No. 1 siRNA | Invitrogen | Cat# 4390843 |
| Silencer Select GLS siRNA | Invitrogen | siRNA ID# s5838 |
| Silencer Select GLS siRNA | Invitrogen | siRNA ID# s5840 |
| Silencer Select GLS2 siRNA | Invitrogen | siRNA ID# s25940 |
| Silencer Select GLS2 siRNA | Invitrogen | siRNA ID# s25941 |
| Silencer Select GATA3 siRNA | Invitrogen | siRNA ID# s5600 |
| Silencer Select GATA3 siRNA | Invitrogen | siRNA ID# s533216 |
| Recombinant DNA | | |
| pCDNA3.1-GAC-myc | This paper | N/A |
| pCDNA3.1-GLS2-HA | This paper | N/A |
| pCDNA3.1-GAC-V5 | This paper | N/A |
| pCDNA3.1-GLS2-V5 | This paper | N/A |
| pQE80-GAC-72–598 | Huang et al., 2018 | N/A |
| pQE80-GLS2-38-602 | Huang et al., 2018 | N/A |
| pCMV-dR8.2 | pCMV delta R8.2 was a gift from Didier Trono | Addgene plasmid #12263 |
| pMD2.G | pMD2.G was a gift from Didier Trono | Addgene plasmid #12259 |
| pLKO.1-puro shRNA control plasmid | Sigma-Aldrich | Cat# SHC002 |
| pLKO.1:TRCN0000051135 targeting GLS | Sigma-Aldrich | Clone ID: NM_014905.2–1441s1c1 |
| pLKO.1:TRCN0000298987 targeting GLS | Sigma-Aldrich | Clone ID: NM_014905.3–1475s21c1 |

| REAGENT or RESOURCE | SOURCE | IDENTIFIER |
|---|---|---|
| pLKO.1:TRCN0000051324 targeting GLS2 | Sigma-Aldrich | Clone ID: NM_013267.2–1804s1c1 |
| pLKO.1:TRCN0000051326 targeting GLS2 | Sigma-Aldrich | Clone ID: NM_013267.2–2053s1c1 |
| Software and Algorithms | | |
| ToxID 2.0 | Thermo Fisher Scientific | N/A |
| MetaboAnalyst | McGill University | https://www.metaboanalyst.ca/ |
| SIEVE 2.0 | Thermo Fisher Scientific | N/A |
| EpiDesigner | Agena Bioscience | https://www.epidesigner.com |
| SigmaPlot | Systat Software Inc | http://www.sigmaplot.co.uk |
| ImageJ | NIH | https://imagej.nih.gov |
| Other | | |
| RPMI 1640 Medium | GIBCO | Cat# 11875093 |
| RPMI 1640 Medium, no glutamine | GIBCO | Cat# 21870076 |
| RPMI 1640 Medium, no phenol red | GIBCO | Cat# 11835030 |
| DMEM, high glucose | GIBCO | Cat# 11965092 |
| Opti-MEM Reduced Serum Medium | GIBCO | Cat# 31985088 |
| Fetal Bovine Serum, qualified, USDA-approved regions | GIBCO | Cat# 10437028 |
| Fetal Bovine Serum, dialyzed, US origin | GIBCO | Cat# 26400044 |
| Lipofectamine 2000 Transfection Reagent | Invitrogen | Cat# 11668019 |
| FuGENE 6 Transfection Reagent | Promega | Cat# E2692 |
| BD Matrigel Matrix | BD Biosciences | Cat# 354234 |
| Novex 12% Tris-Glycine Mini Gels | Thermo Fisher Scientific | Cat# XP00120BOX |
| QIAamp DNA Mini Kit | QIAGEN | Cat# 51304 |
| Qproteome Mitochondria Isolation Kit | QIAGEN | Cat# 37612 |
| RNeasy Mini Kit | QIAGEN | Cat# 74104 |
| QIAshredder | QIAGEN | Cat# 79654 |
| Power SYBR Green PCR Master Mix | Thermo Fisher Scientific | Cat# 4367660 |
| Western Lightning Plus-ECL | Perkin-Elmer | Part# NEL105001EA |